Higgs boson properties and supersymmetry: Constraints and sensitivity from the LHC to an e^+e^- collider

A. Arbey,[1,2] M. Battaglia,[2,3] A. Djouadi,[4,5] F. Mahmoudi,[1,2] M. Mühlleitner,[6] and M. Spira[7]

[1]*Université de Lyon, Université Claude Bernard Lyon 1, CNRS/IN2P3,*
Institut de Physique des 2 Infinis de Lyon, UMR 5822, F-69622, Villeurbanne, France
[2]*CERN, CH–1211 Geneva 23, Switzerland*
[3]*Santa Cruz Institute of Particle Physics, University of California, Santa Cruz, California 95064, USA*
[4]*CAFPE and Departamento de Física Teórica y del Cosmos, Universidad de Granada,*
E–18071 Granada, Spain
[5]*NICPB, Rävala pst. 10, 10143 Tallinn, Estonia*
[6]*Institute for Theoretical Physics, Karlsruhe Institute of Technology, 76131 Karlsruhe, Germany*
[7]*Paul Scherrer Institut, CH–5232 Villigen PSI, Switzerland*

The study of the Higgs boson properties offers compelling perspectives for testing the effects of physics beyond the Standard Model and has deep implications for the LHC program and future colliders. Accurate determinations of the Higgs boson properties can provide us with a distinctively precise picture of the Higgs sector, set tight bounds, and predict ranges for the values of new physics model parameters. In this paper, we discuss the constraints on supersymmetry that can be derived by a determination of the Higgs boson mass and couplings. We quantify these constraints by using scans of the 19-parameter space of the so-called phenomenological minimal supersymmetric Standard Model. The fraction of scan points that can be excluded by the Higgs measurements is studied for the coupling measurement accuracies obtained in LHC run 2 and expected for the HL-LHC program and e^+e^- colliders and contrasted with those derived from missing transverse energy searches at the LHC and from dark matter experiments.

I. INTRODUCTION

The discovery [1] of the Higgs boson [2] at the LHC has opened a vast program of studies of its fundamental properties [3], allowing new and intensive tests of the Standard Model (SM) of particle physics as well as indirect and tight constraints on models of new physics beyond it. In this context, supersymmetric models [4–6] were considered for a long time as the most interesting benchmarks for new physics. In these models, the particle spectrum is more than doubled as every SM particle has a partner of different spin and the Higgs sector is extended to contain more states than the sole SM–like Higgs boson that has been observed at the LHC. Although present LHC studies set stringent bounds on the masses of the new particles, to the extent where supersymmetry (SUSY) appears now to be less "natural" than initially thought, it is nevertheless still worthwhile to keep using and studying it as it remains among the best

benchmarks for new physics searches and provides a rich laboratory for testing the SM. The determination of the Higgs boson mass and the measurement of its couplings to SM fermions and gauge bosons with sufficient accuracy have crucial implications for supersymmetry.

Indeed, while in the SM the properties of the Higgs particle are fixed once its mass is determined, the contributions from the extended Higgs sector and those of the additional SUSY particles may shift the couplings of the SM–like neutral Higgs state and hence, its production rates and decay branching fractions. A precision study of the mass and the production and decay rates is thus essential for establishing the mechanism of electroweak symmetry breaking and of mass generation, for exploring the contributions of new physics models to the Higgs sector and for eventually setting constraints on their parameter spaces. These constraints need to be compared to those obtained from direct searches for the heavier Higgs bosons of the theory and for the SUSY particles in channels with missing transverse energy (MET), as the lightest SUSY particle that always appears at the end of the decay chains is stable and undetectable in the model's most popular versions with R-parity conservation.

The bounds from these searches by the LHC experiments are already significant and will extend to heavier and

heavier SUSY particles, if no signal is observed in the next LHC run (run 3) and in the high–luminosity LHC (HL-LHC) program. It is essential to assess the impact of the constraints derived from the Higgs property measurements, which will also improve in accuracy, on those scenarios that survive the tests of the SUSY direct searches. Conversely, it is important to understand how a given accuracy in the Higgs measurements may enable the reconstruction of the new physics model parameters, in the case where deviations from the SM predictions are observed.

The experience gained with the current analyses from the LHC run 2 data provides us with firm guidelines for the evolution of the accuracy of the Higgs measurements and of the bounds from new particle searches with the larger datasets that are expected in the future. In defining the accuracy of the determination of the Higgs properties, systematic uncertainties, both theoretical and parametric, will play an important role and need to be properly accounted for. With results for most of the Higgs decay and production channels of interest now in hand and mass bounds set by a broad variety of SUSY searches, the time for a detailed assessment of the interplay between Higgs physics and SUSY at the LHC and beyond has come.

After the LHC era, including the HL-LHC program, a new e^+e^- collider promises to deliver measurements that are inherently more precise and cover virtually all the Higgs decay channels. The importance of these data and the requirements for their accuracy, to be considered with the full set of LHC measurements and bounds already in hand, need to be precisely evaluated. Several analyses, some comprehensive and others more focused, that address this important issue have appeared quite recently [7].

In this paper, we attempt to answer these questions by considering two approaches. First, we study the relation between the Higgs coupling modifiers, κ_i, and the fundamental SUSY parameters. Then, we explore the sensitivity of the Higgs measurements to SUSY by quantifying the fraction of the scenarios excluded by the Higgs measurements, the constraints on its parameters, but also the sensitivity to their values in case deviations are observed. The study is conducted in the framework of the so-called phenomenological minimal supersymmetric extension of the Standard Model (pMSSM) [8]. The reduction of the viable pMSSM parameter space obtained by imposing the Higgs properties is compared to that derived from direct SUSY searches in the MET channels through the different stages of the LHC program as well as to the bounds derived from flavor physics and dark matter searches.

II. STUDY OF HIGGS PROPERTIES IN THE PMSSM

A. The pMSSM

In the MSSM, two doublets of complex scalar fields of opposite hypercharge, H_u and H_d, are required to break

spontaneously the electroweak symmetry leading to the presence of five Higgs states, two CP-even Higgs bosons h and H, where the former is considered to be the lightest, a CP-odd Higgs state A, and two charged Higgs bosons $H^\pm$. Because of SUSY constraints, the tree-level masses of the various Higgs bosons and their couplings depend only on two input parameters generally taken to be the pseudoscalar Higgs mass M_A and the ratio of the two vacuum expectation values $\tan\beta$. However, many other MSSM parameters will enter the radiative corrections to the Higgs sector, which are known to play an extremely important role [9–15]. In principle, all soft SUSY–breaking parameters, which in general are of $\mathcal{O}(100)$ in addition to those of the SM, become relevant.

Hence, in the most general MSSM, the analysis of the Higgs sector is tremendously complicated. A phenomenologically more viable MSSM framework, the pMSSM, that is easier to use in practice, can be defined by adopting the following three assumptions: first, all soft SUSY–breaking parameters are real, and there is no new source of CP violation, second, the matrices for the sfermion masses and for the trilinear couplings are all diagonal implying no flavor change at tree level, and third, the soft SUSY–breaking masses and trilinear couplings of the first and second sfermion generations are the same at the electroweak symmetry breaking scale. Making these assumptions will lead to only 22 input parameters in the pMSSM:

 (i) $\tan\beta$: the ratio of the two vacuum expectation values (vevs) of the two Higgs doublet fields, which is expected to lie in the range $1 \lesssim \tan\beta \lesssim m_t/m_b$;

 (ii) M_A: the mass of the pseudoscalar Higgs boson that ranges from M_Z to the SUSY–breaking scale;

 (iii) μ: the Higgsino (supersymmetric) mass parameter (which can have both signs);

 (iv) M_1, M_2, M_3: the bino, wino, and gluino mass parameters;

 (v) $m_{\tilde{Q}}, m_{\tilde{t}_R}, m_{\tilde{b}_R}, m_{\tilde{L}}, m_{\tilde{\tau}_R}$: the third generation sfermion mass parameters;

 (vi) A_t, A_b, A_τ: the third generation trilinear couplings.

 (vii) $m_{\tilde{q}}, m_{\tilde{u}_R}, m_{\tilde{d}_R}, m_{\tilde{l}}, m_{\tilde{e}_R}$: the first and second generation sfermion mass parameters;

 (viii) A_u, A_d, A_e: the first and second generation trilinear couplings;

The first and second generation trilinear couplings A_u, A_d, and A_e will only play a minor role in general and can be ignored in most cases (and, if it is not the case, they can be equated to those of the third generation) so that at the end, one would have 19 basic parameters in practice. This gives the model more predictability and offers an adequate framework for extensive phenomenological studies.

B. Higgs masses and couplings

Let us now come back to the MSSM Higgs sector and discuss the Higgs masses and mixing angles. In the

basis (H_d, H_u), the CP even Higgs mass matrix can be written as[1]

$$\mathcal{M}^2 = M_Z^2 \begin{pmatrix} c_\beta^2 & -s_\beta c_\beta \\ -s_\beta c_\beta & s_\beta^2 \end{pmatrix} + M_A^2 \begin{pmatrix} s_\beta^2 & -s_\beta c_\beta \\ -s_\beta c_\beta & c_\beta^2 \end{pmatrix} + \begin{pmatrix} \Delta\mathcal{M}_{11}^2 & \Delta\mathcal{M}_{12}^2 \\ \Delta\mathcal{M}_{12}^2 & \Delta\mathcal{M}_{22}^2 \end{pmatrix}, \qquad (1)$$

where we use the short-hand notation $s_\beta \equiv \sin\beta$ etc. and introduce the radiative corrections through the general 2×2 matrix $\Delta\mathcal{M}_{ij}^2$. The masses of the neutral CP even h, H bosons and the mixing angle α that diagonalizes the two states can then be written as

$$M_{h/H}^2 = \frac{1}{2}(M_A^2 + M_Z^2 + \Delta\mathcal{M}_+^2 \mp N), \qquad (2)$$

$$\tan\alpha = \frac{2\Delta\mathcal{M}_{12}^2 - (M_A^2 + M_Z^2)s_\beta}{\Delta\mathcal{M}_-^2 + (M_Z^2 - M_A^2)c_{2\beta} + N}, \qquad (3)$$

with

$$\Delta\mathcal{M}_{\pm}^2 = \Delta\mathcal{M}_{11}^2 \pm \Delta\mathcal{M}_{22}^2,$$
$$N = \sqrt{M_A^4 + M_Z^4 - 2M_A^2 M_Z^2 c_{4\beta} + C},$$
$$C = 4\Delta\mathcal{M}_{12}^4 + (\Delta\mathcal{M}_-^2)^2 - 2(M_A^2 - M_Z^2)$$
$$\times \Delta\mathcal{M}_-^2 c_{2\beta} - 4(M_A^2 + M_Z^2)\Delta\mathcal{M}_{12}^2 s_{2\beta}. \qquad (4)$$

The leading radiative corrections to the Higgs mass matrix of Eq. (1) are controlled by the top Yukawa coupling, $\lambda_t = m_t/v\sin\beta$ with $v = 246$ GeV, which appears with the second power accompanied by two additional powers of the top mass. We obtain a very simple analytical expression for the correction matrix $\Delta\mathcal{M}_{ij}^2$ at one-loop if only this contribution is taken into account [9],

$$\Delta\mathcal{M}_{11}^2 \sim \Delta\mathcal{M}_{12}^2 \sim 0,$$
$$\Delta\mathcal{M}_{22}^2 \sim \frac{3\bar{m}_t^4}{2\pi^2 v^2 \sin^2\beta}\left[\log\frac{M_S^2}{\bar{m}_t^2} + \frac{X_t^2}{M_S^2}\left(1 - \frac{X_t^2}{12M_S^2}\right)\right], \qquad (5)$$

where M_S is the geometric average of the two stop masses $M_S = \sqrt{m_{\tilde{t}_1} m_{\tilde{t}_2}}$ defined to be the SUSY–breaking

---

[1]If the SUSY scale is very large, the evolution from this very high scale down to the electroweak scale could mix the quartic couplings of the MSSM Higgs sector in a nontrivial way such that the structure of the mass matrix at the low energy scale could be different from this expression. However, detailed studies in an effective two Higgs doublet model, that is renormalization group improved to resum the large logarithms involving the SUSY–breaking scale, suggest that this assumption is justified in most cases [15].

scale and X_t is the stop mixing parameter given by $X_t = A_t - \mu/\tan\beta$ and $\bar{m}_t$ is the running $\overline{\text{MS}}$ top quark mass at the scale M_S to account for the leading two-loop QCD corrections in a renormalization-group improved approach.

Other SUSY parameters than X_t such as μ and A_b, and, in general, the corrections controlled by the bottom Yukawa coupling $\lambda_b = m_b/v\cos\beta$ as well as the gaugino mass parameters $M_{1,2,3}$, provide a small but non-negligible correction to $\Delta\mathcal{M}_{ij}^2$ and can also have an impact on the loop corrections [10–12,14].

At tree level, the lightest h boson mass is bounded by $M_h \leq M_Z|\cos 2\beta| \leq M_Z \approx 91$ GeV and is thus far from the measured value at the LHC, $M_h = 125.09 \pm 0.24$ GeV [3]. The radiative corrections have therefore to be rather large in order to attain this value. In the leading one-loop approximation above, the maximal value mass $M_h^{\max}$ is given by

$$M_h^2 \overset{M_A \gg M_Z}{\longrightarrow} M_Z^2 \cos^2 2\beta + \Delta\mathcal{M}_{22}^2 s_\beta^2, \qquad (6)$$

and is obtained for the following choice of SUSY parameters [16]: (i) a decoupling regime with heavy A states, $M_A \sim \mathcal{O}(\text{TeV})$ in order to minimize Higgs mixing; (ii) large values of the parameter $\tan\beta$, $\tan\beta \gtrsim 10$, in order to maximize the tree-level contribution $M_Z|\cos 2\beta|$; (iii) heavy stop squarks, i.e., large M_S values to enhance the logarithmic contributions; (iv) a stop trilinear coupling of $X_t = \sqrt{6}M_S$, the so-called maximal mixing scenario that maximizes the stop loops [16]. If the parameters are optimized as above, the maximal M_h value can then reach the level of the measured value $M_h = 125$ GeV for $M_S > 1$ TeV.

The basic feature of the hMSSM approach [17–19], that we will adopt in most cases for our effective Higgs coupling study, is that we can trade the radiative correction $\Delta\mathcal{M}_{22}^2$ of Eq. (5) for the measured Higgs mass value $M_h = 125$ GeV. In this case, the MSSM Higgs sector with solely the dominant radiative corrections included, can be again described with only two unknown parameters, such as $\tan\beta$ and M_A as it was the case at tree-level. The dominant radiative corrections involving the SUSY parameters are fixed by the value of M_h. This observation leads to a rather simple and accurate[2] parametrization of the MSSM Higgs sector and, more specifically, the heavier CP-even Higgs mass and the CP-even mixing angle can be expressed in terms of M_A, M_h, and $\tan\beta$ as

---

[2]If the SUSY scale is not extremely high, the approach would need some refinements at high values of $\tan\beta$ and μ to describe properly the Yukawa couplings to bottom quarks and τ leptons as will be discussed later. In addition, there are subleading contributions to the Higgs mass matrix other than $\Delta\mathcal{M}_{22}^2$, but these have been shown to be rather small as will also be discussed.

$$M_H^2 = \frac{(M_A^2 + M_Z^2 - M_h^2)(M_Z^2 c_\beta^2 + M_A^2 s_\beta^2) - M_A^2 M_Z^2 c_{2\beta}^2}{M_Z^2 c_\beta^2 + M_A^2 s_\beta^2 - M_h^2},$$

$$\alpha = -\arctan\left(\frac{(M_Z^2 + M_A^2)c_\beta s_\beta}{M_Z^2 c_\beta^2 + M_A^2 s_\beta^2 - M_h^2}\right). \tag{7}$$

The mass of the charged Higgs state $M_{H^\pm}$ is simply given by the tree-level relation,

$$M_{H^\pm}^2 = M_A^2 + M_W^2, \tag{8}$$

as the SUSY radiative corrections in this particular case are known to be small [20]. We can now discuss the production and decay rates of the MSSM Higgs bosons, restricting for the moment to the SM-like one h.

C. h production and decays

In many respects, we are fortunate enough as the mass value of $M_h = 125$ GeV of the SM–like h particle allows us to produce the state in several redundant channels and to detect it in a variety of decay modes.

First, many production processes have significant rates for a light SM-like Higgs boson. The by far dominant gluon fusion mechanism,

$$gg \to h$$

that we will denote ggh, develops a large cross section for $M_h = 125$ GeV, $\sigma_{\mathrm{ggh}}^{\mathrm{tot}} \approx 50$ pb at $\sqrt{s} = 14$ TeV. For such a Higgs mass, the subleading channels, i.e., the vector boson fusion (VBF) process,

$$qq \to hqq$$

and the Higgs–strahlung (hV) mechanisms,

$$q\bar{q} \to hV$$

with $V = W$, Z, have cross sections at $\sqrt{s} = 14$ TeV that are of the order of, respectively, $\sigma_{\mathrm{VBF}}^{\mathrm{tot}} \approx 4$ pb and $\sigma_{\mathrm{hV}}^{\mathrm{tot}} \approx 2.5$ pb when the two channels hZ and hW are combined. These rates would lead to large samples that would allow for a detailed study of the Higgs particle with the large amount of integrated luminosity, $\mathcal{L} \approx 3000$ fb^{-1}, that is expected to be collected at the high–luminosity option of the LHC (HL–LHC). Even the associated Higgs production with top quark pairs (tth),

$$pp \to t\bar{t}h$$

with a cross section of $\sigma_{\mathrm{tth}}^{\mathrm{tot}} \approx 0.6$ pb and, to a much lesser extent, double Higgs production in the dominant gluon–fusion channel (gghh),

$$gg \to hh$$

with a cross section of $\sigma_{\mathrm{gghh}}^{\mathrm{tot}} \approx 50$ fb could be probed with such a high luminosity.

Second, for $M_h = 125$ GeV, the Higgs boson mainly decays into $b\bar{b}$ pairs,

$$h \to b\bar{b}$$

with a branching ratio of $\approx 60\%$, but the decays into massive gauge boson final states,

$$h \to WW^* \quad \text{and} \quad ZZ^*$$

before allowing the gauge bosons to decay leptonically $W \to \ell\nu$ and $Z \to \ell\ell$ ($\ell = e, \mu$), are also significant with branching ratios of $\approx 20\%$ and 2.5%, respectively. The leptonic decay channel,

$$h \to \tau^+\tau^-$$

is also of significance with a branching fraction of $\approx 5\%$ as is the case for the $h \to gg$ ($\approx 8\%$) and $h \to c\bar{c}$ ($\approx 3\%$) decay modes (that are not detectable at the LHC to first approximation). The clean loop induced decay mode,

$$h \to \gamma\gamma$$

can be easily detected albeit its small branching ratio of 2×10^{-3}. Even the rare $h \to \mu^+\mu^-$ decay with a branching fraction of order 2×10^{-4} has provided first evidence in the ATLAS [21] and CMS [22] latest searches, and the $h \to Z\gamma$ channel should be accessible at the HL-LHC.

The branching fractions of the h bosons in our pMSSM scans in the $b\bar{b}$, W^+W^- and ZZ and $\tau^+\tau^-$ decay channels normalized to the SM predictions are shown in Fig. 1. Some of their correlations are given in Fig. 2. They have been obtained with the program HDECAY [23], used in this study to precisely evaluate the various Higgs partial decay widths and branching ratios and show a broad range of variation away from the SM predictions.

D. The invisible Higgs decay width

In many extensions of the SM, the light scalar Higgs boson can decay into pairs of non-SM particles. In the case of the MSSM, Higgs decays into squarks and gluinos are kinematically excluded as present experimental bounds constrain these particles to be much heavier than $\frac{1}{2}M_h$. These decays are also kinematically closed for the charged sleptons, the two charginos, and the three heavier neutralinos as searches from the LEP experiment have set limits beyond 100 GeV on the masses of these particles. Invisible h boson decays are still possible in the context of a fully unconstrained MSSM in which the various soft
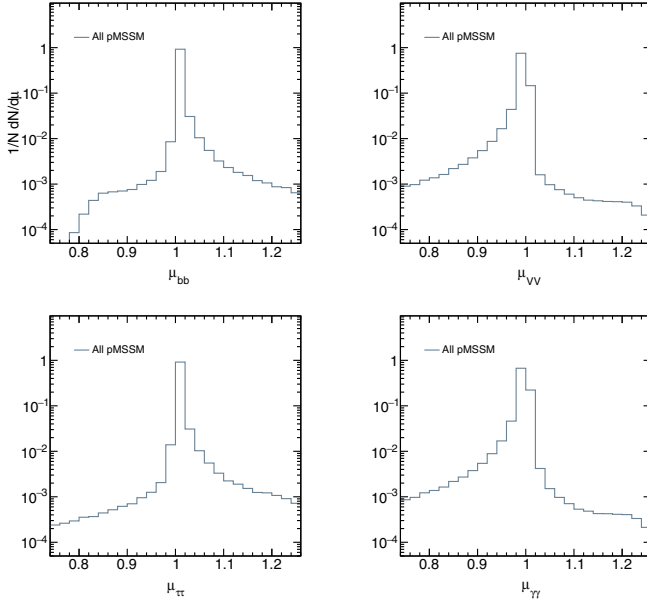
FIG. 1. Distributions of h decay branching fractions normalised to their SM prediction, μ, for the $b\bar{b}$ (top), W^+W^- and ZZ (second from top), $\tau^+\tau^-$ (bottom) and $\gamma\gamma$ (second from bottom) for pMSSM points.

SUSY-breaking parameters are unrelated, and they are of two types.

The first kinematically still possible SUSY mode for the h boson is the decay into a pair of the lightest neutralino χ_1^0 which, in most cases, is the lightest supersymmetric particle (LSP) and is stable if R-parity is conserved. This is largely allowed by present experimental constraints in particular in nonconstrained or nonunified models in which the soft SUSY-breaking gaugino mass parameters M_1, M_2, M_3 are not related and the relatively strong experimental bounds on the masses of the charginos, $m_{\chi_1^\pm} \gtrsim 100$ GeV from LEP2, and the gluino, $m_{\tilde{g}} \approx M_3 \gtrsim 1$ TeV from present LHC searches, do not affect the invisible neutralino, and one could have $m_{\chi_1^0} < \frac{1}{2} M_h$.

The partial width for the invisible Higgs decay into neutralinos is given by

$$\Gamma(h \to \chi_1^0 \chi_1^0) = \frac{G_F M_W^2 M_h}{2\sqrt{2}\pi} g_{h\chi_1^0\chi_1^0}^2 \beta_\chi^3, \qquad (9)$$

with the neutralino velocity being $\beta_\chi = (1 - 4m_{\chi_1^0}^2/M_h^2)^{1/2}$ and the normalized Higgs-neutralino coupling given by

$$g_{h\chi_1^0\chi_1^0} = (Z_{12} - \tan\theta_W Z_{11})(\sin\beta Z_{14} - \cos\beta Z_{13}),$$

where Z is the 4×4 matrix that diagonalizes the neutralino mass matrix [6]. The decay is important only for moderate and comparable values of the bino mass parameter M_1 and the Higgsino parameter μ: moderate $M_1 \lesssim \mathcal{O}(60 \text{ GeV})$ to have a light enough LSP as one has $m_{\chi_1^0} \approx M_1$ for
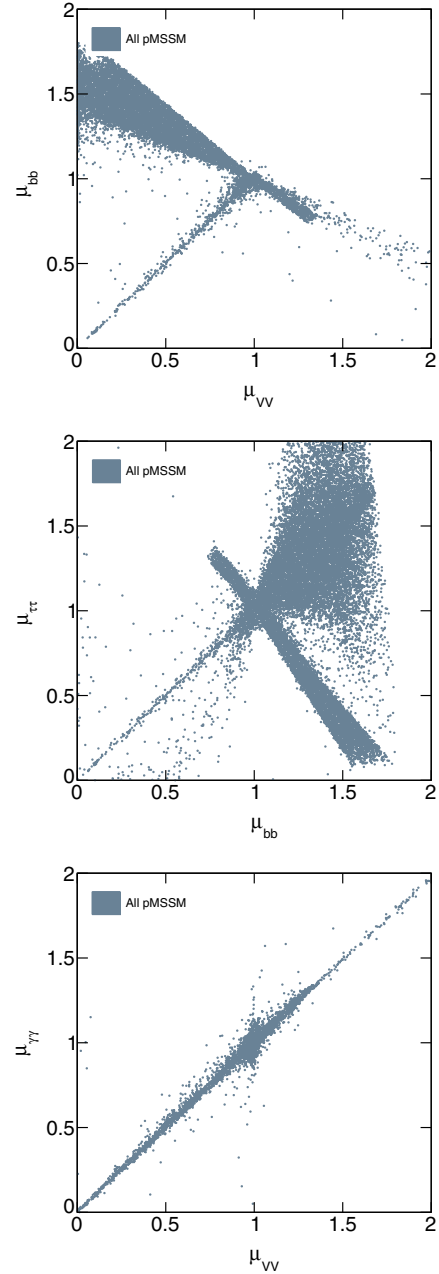

FIG. 2. Distributions of the correlations between pairs of the h decay branching fractions normalized to their SM predictions for pMSSM points.

$M_1 \lesssim |\mu|, M_2$ and comparable values $|\mu| = \mathcal{O}(M_1)$ as the h boson prefers to couple to neutralinos, which are a mixture of gauginos and Higgsinos,[3] $Z_{13}, Z_{14} = \mathcal{O}(1)$. In this parameter range, the decay $h \to \chi_1^0 \chi_1^0$ can be substantial if M_h is above the $2m_{\chi_1^0}$ threshold; close to this value, the width is strongly suppressed by the β_χ^3 velocity factor.

---

[3]Note, however, that the LEP2 bound on the lightest chargino mass forces the parameters M_2 and μ to be somewhat large, $\min(|\mu|, M_2) \approx m_{\chi_1^\pm} \gtrsim 100$ GeV.

The neutralino LSP with such a mass would have the relic density required by PLANCK results for Ω_{CDM}, since it will annihilate efficiently through the exchange of the h boson [24]. However, in this case, the invisible branching fraction should be relatively small, $\mathrm{BR}(h \to \chi_1^0 \chi_1^0) \lesssim \mathcal{O}(10\%)$ as discussed, for instance, in Ref. [25].

Scenarios in which μ and M_1 are small enough to lead to a light LSP with reasonable couplings to the h boson would lead to large rates for chargino-neutralino pair production at the LHC (in particular, a large amount of trilepton events from the process $q\bar{q} \to W^* \to \chi_1^\pm \chi_i^0 \to W Z \chi_1^0 \chi_1^0 \to 3\ell^\pm + E_T^{\mathrm{mis}}$). However, because these states have rather compressed spectra, with the $\chi_1^\pm, \chi_i^0$ masses too close to that of the LSP, the missing energy is small and the process could escape observation at the LHC.

Another, albeit less likely, possibility would be that the Higgs boson decays into a pair of sneutrinos which, if they are lighter than the chargino $\chi_1^\pm$ and the second neutralino χ_2^0 and the sleptons, would have as only possible decay the channel $\tilde{\nu} \to \nu \chi_1^0$ with χ_1^0 the LSP and the decay is thus also invisible. As the experimental lower bound on the $\tilde{\nu}$ masses is rather low, $m_{\tilde{\nu}} \gtrsim 45$ GeV from the invisible Z decay width [26], there is a tight room $\frac{1}{2}M_Z \lesssim m_{\tilde{\nu}} \lesssim \frac{1}{2}M_h$, for the decay $h \to \tilde{\nu}\tilde{\nu}$ to occur. However, as a result of $\mathrm{SU}(2)_{\mathrm{L}}$ invariance, the soft SUSY-breaking sneutrino and left-handed charged slepton mass parameters are related and to cope with the bound on slepton masses from LEP2 searches, $m_{\tilde{l}} \gtrsim 90$ GeV, the mass $m_{\tilde{\nu}_L}$ should be high enough. Nevertheless, a small room is still possible for relatively light sneutrino as a splitting between $\tilde{\nu}$ and $\tilde{l}_L$ masses can be generated by the D terms which, for small values of the common scalar mass $\tilde{m}$ and for large $\tan\beta$ values for which they become maximal, govern the slepton masses (note that additional significant contributions to the D terms could arise beyond the MSSM). As these D terms tend to increase $m_{\tilde{\ell}_L}$ and decrease $m_{\tilde{\nu}}$, sneutrino masses $m_{\tilde{\nu}} \lesssim \frac{1}{2}M_h$ can be obtained while keeping the $m_{\tilde{\ell}} \gtrsim 90$ GeV experimental constraint still valid.

The partial width for the decay mode, summing over the three possible sneutrinos, is given by

$$\Gamma(h \to \tilde{\nu}\tilde{\nu}) = \frac{3 G_F M_Z^4}{8\sqrt{2}\pi M_h} g_{h\tilde{\nu}\tilde{\nu}}^2 \beta_{\tilde{\nu}}, \quad \beta_{\tilde{\nu}} = \left[1 - \frac{4m_{\tilde{\nu}}^2}{M_h^2}\right]^{1/2} \quad (10)$$

The h boson coupling to sneutrinos, $g_{h\tilde{\nu}\tilde{\nu}} \propto \cos 2\beta$ in the decoupling limit, is also maximal at high $\tan\beta$ and is much larger than the bottom-quark Yukawa coupling, making the partial width huge. When the decay is not kinematically suppressed, it would dominate all other decays in contrast to current LHC observation. If the possibility of light sneutrinos is to hold, one thus needs to strongly suppress this decay channel and bring it at the few 10% level at most. Two possibilities are then at hand. A first

one is that the sneutrino mass is close to the kinematical threshold $m_{\tilde{\nu}} \approx \frac{1}{2} M_h^2$ so that the partial decay width in Eq. (10) is strongly suppressed by the sneutrino velocity $\beta_{\tilde{\nu}}$. A second possibility would be to suppress the $h\tilde{\nu}\tilde{\nu}$ couplings and hence, adopt a value of $\tan\beta$ that is very close to unity for which $\cos 2\beta \to 0$. Both options can coexist of course.

Another possibility would be Higgs decays into the very light gravitinos and the next-to-LSP neutralino χ_1^0 in gauge mediated SUSY–breaking models, $h \to \chi_1^0 \tilde{G}$, with a very long-lived next-to-LSP that decays outside the detector making the photon in the decay $\chi_1^0 \to \tilde{G}\gamma$ unobservable. However, for the $h \to \chi_1^0 \tilde{G}$ rate to be substantial, the scale for SUSY-breaking should be rather low, and this is already excluded in most realistic scenarios [27]. Nevertheless, one should keep this possibility in mind in more complex models.

Concretely, all these cases can be parametrized by an invisible Higgs partial width,

$$\Delta_{\mathrm{inv}} = \Gamma_h^{\mathrm{inv}}/\Gamma_h^{\mathrm{tot}} = \Gamma(h \to \mathrm{invisible})/\Gamma_{\mathrm{SM}}(h \to \mathrm{all}). \quad (11)$$

For scenarios where the decay channel is open, the rate into invisible particles is expected to be mostly at the few percent to the 10% level, and they cannot yet be excluded by the LHC data [28–31].

E. Direct corrections to the Higgs couplings

Higgs decays into quark pairs are strongly affected by (SUSY-)QCD corrections, while (SUSY-)electroweak corrections are in general of moderate size [32,33]. The dominant part of the QCD corrections to the decays into bottom and charm quarks can be absorbed in the running Yukawa coupling if it is evaluated at the scale of the Higgs mass [34]. This requires the introduction of the running quark masses that are defined in the $\overline{\mathrm{MS}}$ scheme in the program HDECAY [23]. The pure QCD corrections beyond the running-mass effects are included up to N⁴LO [34]. The SUSY-QCD corrections mediated by gluino-squark exchange are fully known up to NLO [33,35] and included in HDECAY. The dominant part of the SUSY-QCD and SUSY–electroweak corrections in the Higgs decays into bottom quarks can be approximated by the Δ_b terms that at one-loop order are given by [36–38]

$$\Delta_b = \Delta_b^{\mathrm{QCD}} + \Delta_b^{\mathrm{EW},t} + \Delta_b^{\mathrm{EW},1} + \Delta_b^{\mathrm{EW},2}, \quad (12)$$

with the individual contributions,

$$\Delta_b^{\mathrm{QCD}} = \frac{2}{3}\frac{\alpha_s}{\pi} m_{\tilde{g}}\mu\tan\beta I(m_{\tilde{b}_1}^2, m_{\tilde{b}_2}^2, m_{\tilde{g}}^2),$$

$$\Delta_b^{\mathrm{EW},t} = \frac{\lambda_t^2}{(4\pi)^2} A_t\mu\tan\beta I(m_{\tilde{t}_1}^2, m_{\tilde{t}_2}^2, \mu^2),$$

$$\Delta_b^{\mathrm{EW},1} = -\frac{\alpha_1}{12\pi} M_1\mu\tan\beta\Big\{\frac{1}{3}I(m_{\tilde{b}_1}^2, m_{\tilde{b}_2}^2, M_1^2)$$
$$+ \left(\frac{c_b^2}{2} + s_b^2\right)I(m_{\tilde{b}_1}^2, M_1^2, \mu^2)$$
$$+ \left(\frac{s_b^2}{2} + c_b^2\right)I(m_{\tilde{b}_2}^2, M_1^2, \mu^2)\Big\},$$

$$\Delta_b^{\mathrm{EW},2} = -\frac{\alpha_2}{4\pi} M_2\mu\tan\beta\Big\{c_t^2 I(m_{\tilde{t}_1}^2, M_2^2, \mu^2) + s_t^2 I(m_{\tilde{t}_2}^2, M_2^2, \mu^2),$$
$$+ \frac{c_b^2}{2}I(m_{\tilde{b}_1}^2, M_2^2, \mu^2) + \frac{s_b^2}{2}I(m_{\tilde{b}_2}^2, M_2^2, \mu^2)\Big\}, \qquad (13)$$

where α_s denotes the strong coupling, $\lambda_t = \sqrt{2}m_t/(v\sin\beta)$ the top Yukawa coupling, $\alpha_1 = g'^2/4\pi$ and $\alpha_2 = g^2/4\pi$ the electroweak gauge couplings. The masses $m_{\tilde{g}}, m_{\tilde{b}_{1,2}}$, and $m_{\tilde{t}_{1,2}}$ are the gluino, sbottom, and stop masses. The terms $s/c_{t,b} = \sin/\cos\theta_{t,b}$ are related to the stop/sbottom mixing angles $\theta_{t,b}$. The generic function I is defined as

$$I(a, b, c) = \frac{ab\log\frac{a}{b} + bc\log\frac{b}{c} + ca\log\frac{c}{a}}{(a-b)(b-c)(a-c)}. \qquad (14)$$

The corresponding Δ_τ term for the tau-lepton couplings acquires contributions from the EW gauge couplings α_1 and α_2 only. These are given by [36]

$$\Delta_\tau = \Delta_\tau^{\mathrm{EW},1} + \Delta_\tau^{\mathrm{EW},2}, \qquad (15)$$

with the individual contributions,

$$\Delta_\tau^{\mathrm{EW},1} = \frac{\alpha_1}{4\pi} M_1\mu\tan\beta\Big\{I(m_{\tilde{\tau}_1}^2, m_{\tilde{\tau}_2}^2, M_1^2) + \left(\frac{c_\tau^2}{2} - s_\tau^2\right)$$
$$\times I(m_{\tilde{\tau}_1}^2, M_1^2, \mu^2) + \left(\frac{s_\tau^2}{2} - c_\tau^2\right)I(m_{\tilde{\tau}_2}^2, M_1^2, \mu^2)\Big\},$$

$$\Delta_\tau^{\mathrm{EW},2} = -\frac{\alpha_2}{4\pi} M_2\mu\tan\beta\Big\{I(m_{\tilde{\nu}_\tau}^2, M_2^2, \mu^2)$$
$$+ \frac{c_\tau^2}{2}I(m_{\tilde{\tau}_1}^2, M_2^2, \mu^2) + \frac{s_\tau^2}{2}I(m_{\tilde{\tau}_2}^2, M_2^2, \mu^2)\Big\}, \qquad (16)$$

where $s/c_\tau = \sin/\cos\theta_\tau$ is related to the $\tilde{\tau}$ mixing angle θ_τ and $m_{\tilde{\tau}_{1,2}}, m_{\tilde{\nu}_\tau}$ denote the stau and tau sneutrino masses, respectively.

These $\Delta_f(f = b, \tau)$ terms modify the effective bottom and τ Yukawa couplings $\tilde{g}_f^\phi(\phi = h, H, A)$ of the two neutral CP-even states h, H and the CP-odd state A, as follows [37,38][4]:

---

[4]Analogous corrections emerge for the muon and strange Yukawa couplings, but they do not play a role in our analysis.

$$\tilde{g}_f^h = \frac{g_f^h}{1 + \Delta_f}\left[1 - \frac{\Delta_f}{\tan\alpha\tan\beta}\right],$$

$$\tilde{g}_f^H = \frac{g_f^H}{1 + \Delta_f}\left[1 + \Delta_f\frac{\tan\alpha}{\tan\beta}\right],$$

$$\tilde{g}_f^A = \frac{g_f^A}{1 + \Delta_f}\left[1 - \frac{\Delta_f}{\tan^2\beta}\right], \qquad (17)$$

in terms of the original Yukawa couplings g_f^ϕ,

$$g_u^h = \frac{\cos\alpha}{\sin\beta}, \qquad g_d^h = -\frac{\sin\alpha}{\cos\beta},$$
$$g_u^H = \frac{\sin\alpha}{\sin\beta}, \qquad g_d^H = \frac{\cos\alpha}{\cos\beta},$$
$$g_u^A = \cot\beta, \qquad g_d^A = \tan\beta, \qquad (18)$$

for up- and down-type fermions, where α is the mixing angle of the neutral CP-even Higgs states. It has been shown that the effective bottom Yukawa couplings absorb the bulk of the SUSY-QCD and -EW corrections to most of the production and decay processes mediated by these couplings up to a remainder of a few percent, while the full SUSY–QCD corrections can reach about 100%. The two-loop QCD corrections to Δ_b have been calculated and shown to add a moderate correction of about 10% [39]. They are included in HDECAY [23] thus increasing the reliability of the predictions even in cases of large Δ_b terms.

Similarly to the isospin down-type fermions, direct corrections also affect the $ht\bar{t}$ couplings. Contrary to the terms discussed so far, these are suppressed by $\tan\beta$ and hence, can be important only at very low $\tan\beta$, $\tan\beta \approx 1$. The corresponding Δ_t correction is given by

$$\Delta_t = \mu\cot\beta\left[\frac{2\alpha_s}{3\pi}m_{\tilde{g}}I(m_{\tilde{t}_1}^2, m_{\tilde{t}_2}^2, m_{\tilde{g}}^2)\right.$$
$$\left. + \frac{\lambda_b^2}{(4\pi)^2}A_b I(m_{\tilde{b}_1}^2, m_{\tilde{b}_2}^2, \mu^2)\right], \qquad (19)$$

and hence, only the first term would contribute since $\lambda_b = \sqrt{2}m_b/(v\cos\beta)$ is small as there is no relative enhancement by $\tan\beta$ values. However, for the same reason, these corrections turn out to be small in total as they are not enhanced by $\tan\beta$ factors at all.

For the decays into photon pairs, the additional SUSY-loop contributions mediated by chargino, sfermion, and charged Higgs loops are taken into account. In this way, a significant dependence on the SUSY parameters is induced that can lead to sizeable modifications of the corresponding partial width from the SM expression, if SUSY particles are relatively light. The QCD and EW corrections are small for the light scalar Higgs decay into photons [40,41]. Similar features also apply to the less relevant Higgs decays into $Z\gamma$ [42] and, for the EW corrections, into gg [43]. In the latter

case of gluonic decays, the QCD corrections are large [44], however, and are included in HDECAY [23]. The QCD and EW corrections to the $H \rightarrow Z\gamma$ decay width are not included in HDECAY.

Within the MSSM there are novel Higgs decays as, e.g., the heavy scalar Higgs decay into a pair of two light *CP*-even Higgs bosons $H \rightarrow hh$ that plays a role for small values of $\tan\beta$ below the $t\bar{t}$ threshold [45]. Higher order corrections to this decay mode are only taken into account for the effective trilinear Higgs coupling, obtained in the framework of the RG-improved effective potential, while process-dependent corrections are not included [46].

Finally, the MSSM Higgs bosons can also decay into SUSY particles where the partial decay widths into final states with charginos and neutralinos may be significant for the heavier Higgs particles [47]. The possibility of the light scalar Higgs decay into a pair of neutralinos is reduced to very small and exceptional regions of the MSSM parameter space and is thus not of relevance for our study as discussed in Sec. II D. Higgs decays into sfermion pairs may only play a role for the heavy Higgs bosons but not for the light scalar h [47] in the context of the present LHC bounds on the sfermion masses (except for sneutrinos as discussed before).

The MSSM Higgs sector is implemented in HDECAY [23] within the renormalization group-improved effective potential approach, including the dominant top- and bottom-Yukawa coupling induced two-loop corrections. The residual uncertainties of this approach on the light scalar Higgs mass amount to about 3–5 GeV, depending on the MSSM scenario. The same perturbative level is also extended to the trilinear and quartic Higgs self-couplings by modifying the official version of the subh subroutine of Refs. [10] accordingly. The present state-of-the-art calculations for the Higgs masses include partial three-loop corrections that reduce the uncertainty on the light scalar Higgs mass to a level of 1–2 GeV [48]. These latter contributions are not included in HDECAY.

F. Coupling modifiers and effective Higgs couplings

The deviations of Higgs production cross sections and decay branching fractions from the SM predictions due to new physics contributions can be analyzed in terms of coupling-modifier terms, κ_X, in the context of the so-called κ-framework formalism [49]. The factors κ_X for a particle X are defined as

$$\kappa_X = g^{\mathrm{MSSM}}_{hXX}/g^{\mathrm{SM}}_{H_{\mathrm{SM}}XX}, \qquad (20)$$

so that the h cross sections and partial decay widths to the particle type X, normalized to the ones of the SM Higgs particle H_{SM}, scale as κ_X^2.

It must be stressed that, under these assumptions, only the Higgs boson couplings of processes existing in the SM are modified by new physics and possible modifications to

the kinematics of the production and decay processes are not considered. This is justified in the context of the pMSSM with the lightest neutralino χ_1^0 being the LSP, provided that $M_{\chi_1^0} > \frac{1}{2}M_h$ so that decays to any SUSY particle are kinematically forbidden.

The relations between the coupling modifiers κ_X and the SUSY parameters can also be discussed in the context of the so-called hMSSM approach. This has been shown to be a good approximation to the full MSSM, since its basic underlying assumption, that the radiative corrections to the Higgs mass matrix of Eq. (1) are dominated by the $\Delta\mathcal{M}_{22}^2$ entry, is verified in most cases.[5]

The MSSM couplings normalized to their SM-like values, $c_X^0 = g^{\mathrm{MSSM}}_{hXX}/g^{\mathrm{SM}}_{hXX}$, correspond to the κ_X modifiers when all direct radiative corrections are neglected. These values for the couplings of the light h state to third generation t, b fermions and $V = W/Z$ gauge bosons, including the radiative corrections entering in the MSSM Higgs masses and mixing only, are given by

$$c_V^0 = \sin(\beta - \alpha), \qquad c_t^0 = g_u^h, \qquad c_b^0 = g_d^h, \quad (21)$$

with the couplings g_u^h and g_d^h of Eq. (18) and the angle α given by Eq. (7). In the decoupling regime with a heavy pseudoscalar Higgs boson, $M_A \gg M_Z$, the mixing angle α gets close to $\alpha \approx \beta - \frac{\pi}{2}$ making the h couplings to fermions and massive gauge bosons SM-like, namely $c_V^0, c_t^0, c_b^0 \rightarrow 1$.

In this limit, the heavier *CP*-even and the charged Higgs states become almost degenerate in mass with the *CP*-odd A boson, $M_H \approx M_{H^\pm} \approx M_A \gg M_h$, while the couplings of the neutral H and A states become similar. In particular, there are no more H couplings to the weak bosons as is the case for the state A by virtue of *CP* invariance,

$$g_{HVV} = \sqrt{1 - (c_V^0)^2} = \cos(\beta - \alpha)$$
$$\xrightarrow{M_A \gg M_Z} 0 \equiv g_{AVV} \qquad (22)$$

In fact, the magnitude of the coupling g_{HVV} is a very good measure of the decoupling limit in which the h couplings are SM–like. Performing an expansion in terms of the inverse pseudoscalar Higgs mass, one obtains in the approach to this limit,

$$g_{HVV} \xrightarrow{M_A \gg M_Z} \chi \equiv \frac{1}{2}\frac{M_Z^2}{M_A^2}\sin 4\beta - \frac{1}{2}\frac{\Delta\mathcal{M}_{22}^2}{M_A^2}\sin 2\beta, \qquad (23)$$

---

[5]In Ref. [17], the impact of the subleading corrections $\Delta\mathcal{M}_{11}^2$ and $\Delta\mathcal{M}_{12}^2$ has been proven to be small via a scan of the MSSM parameter space (in particular, the parameters $\mu, A_t, A_b, M_1, M_2, M_3$, and M_S) in which the full radiative corrections to the Higgs sector up to two loops are implemented. Several other independent analyses [19,50] have reached the same conclusions.

where the first term is due to the tree-level contribution and the second one to the dominant contribution of the radiative corrections. A look at the tree-level component shows that for both large $\tan\beta$ and $\tan\beta$ values close to unity, the decoupling limit is reached more quickly as the expansion parameter involves the factor $\sin 4\beta$ which, in the two limiting cases, behaves as

$$\sin 4\beta = \frac{4\tan\beta(1-\tan^2\beta)}{(1+\tan^2\beta)^2}$$
$$\rightarrow \begin{cases} -4/\tan\beta & \text{for } \tan\beta \gg 1 \\ 1-\tan^2\beta & \text{for } \tan\beta \sim 1 \end{cases} \rightarrow 0 \quad (24)$$

and the g_{HVV} coupling is doubly suppressed by both M_Z^2/M_A^2 and $\tan\beta$ terms in these limits. In the radiatively generated component, the one-loop correction $\Delta\mathcal{M}_{22}^2$ of Eq. (5) involves a term that goes like $1/\sin^2\beta$, which makes it proportional to $-\Delta\mathcal{M}_{22}^2/M_A^2 \times \cot\beta$ and thus, vanishes at high $\tan\beta$ values. This leads to the well-known fact that the decoupling limit $g_{HVV} \rightarrow 0$ is reached very quickly in this case, in fact as soon as $M_A \gtrsim 150$–200 GeV.

Instead, for $\tan\beta \approx 1$, this radiatively generated component is maximal. However, when both the tree-level and radiative components are included, the largest departure of the coupling g_{HVV} from zero for a fixed M_A value occurs when $\sin 4\beta \approx -1$. This corresponds to an angle $\beta = 3\pi/8$ and hence to the value $\tan\beta \approx 2.4$.

Similarly to the coupling to gauge bosons, one can write the couplings of the h state to isospin $\frac{1}{2}$ and $-\frac{1}{2}$ fermions in the approach to the decoupling limit as

$$c_t^0 = \sin(\beta-\alpha) + \cot\beta\cos(\beta-\alpha) \xrightarrow{M_A \gg M_Z} 1 + \chi\cot\beta \rightarrow 1$$
$$c_b^0 = \sin(\beta-\alpha) - \tan\beta\cos(\beta-\alpha) \xrightarrow{M_A \gg M_Z} 1 - \chi\tan\beta \rightarrow 1,$$
$$(25)$$

where the expansion parameter $\chi \propto 1/M_A^2$ is the same as the one given in Eq. (23). In the approach to the decoupling limit $M_A \gg M_Z$, the h couplings to bottom (top) quarks have an additional $\tan\beta$ ($\cot\beta$) factor. Hence, at high $\tan\beta$ values, the lightest Higgs couplings to bottom quarks can be different from the SM–one even at high M_A values, contrary to the h couplings to gauge bosons and top quarks. At low $\tan\beta$ values, significant deviations from the decoupling can be observed for all h couplings even for a relatively heavy A state. The couplings to bb and $\tau\tau$ as a function of M_A from our pMSSM scans are compared to the scaling of Eq. (25) with M_A in Fig. 3.

The simple picture of the hMSSM is altered by additional direct radiative corrections. These contributions can be effectively mapped into few parameters and these can, in principle, be isolated experimentally. The most important direct correction occurs in the case of b-quarks where
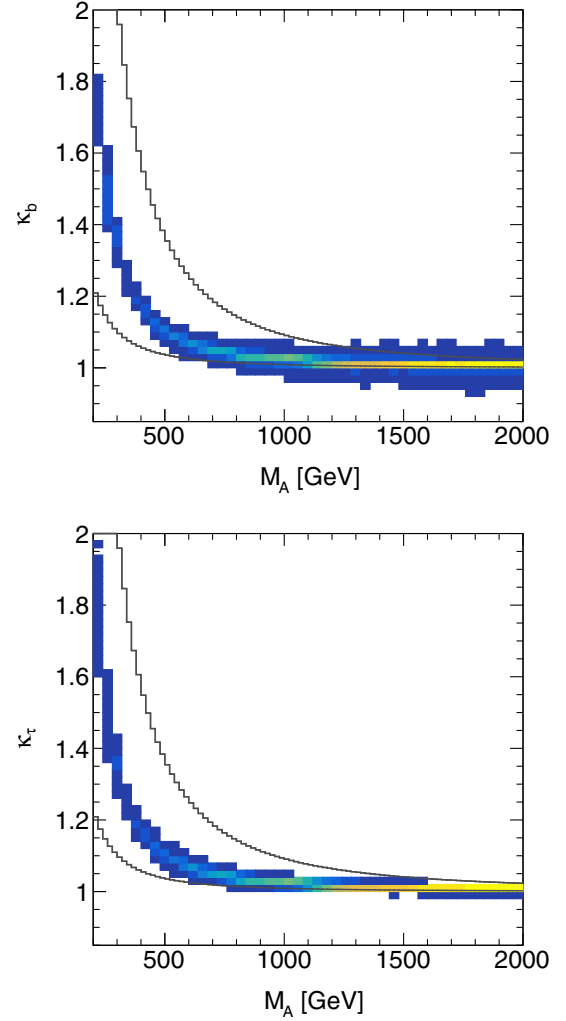

FIG. 3. The variation of the h^0 $b\bar{b}$ (upper) and $\tau\tau$ (lower panel) coupling modifiers as a function of M_A. The histograms are obtained with HDECAY for the valid pMSSM scan points. The lines show the scaling of Eq. (25) with M_A for $M_S = 1000$ GeV, $X_t = 1000$ GeV, and $\tan\beta = 2$ (upper line) and 20 (lower line). The color scale ranges from dark to light according to the increasing fraction of scan points in each bins.

additional one-loop vertex terms modify the tree-level $hb\bar{b}$ coupling outside the decoupling regime. They grow as $\mu\tan\beta$ and are thus very large at high $\tan\beta$. The dominant component comes from the SUSY-QCD corrections in which sbottoms and gluinos are exchanged in the loops, but an important electroweak contribution comes from stop and chargino loops in addition. In the case of the $hb\bar{b}$ coupling, this correction appears only outside the decoupling regime and results in an effective correction term,

$$\kappa_b = \tilde{g}_b^h = c_b^0 \times \frac{1 - \Delta_b \cot\alpha\cot\beta}{1 + \Delta_b} \qquad (26)$$

where the resummation of Eq. (17) has been included. In the decoupling regime, $\tan\alpha$ approaches $-1/\tan\beta$ when
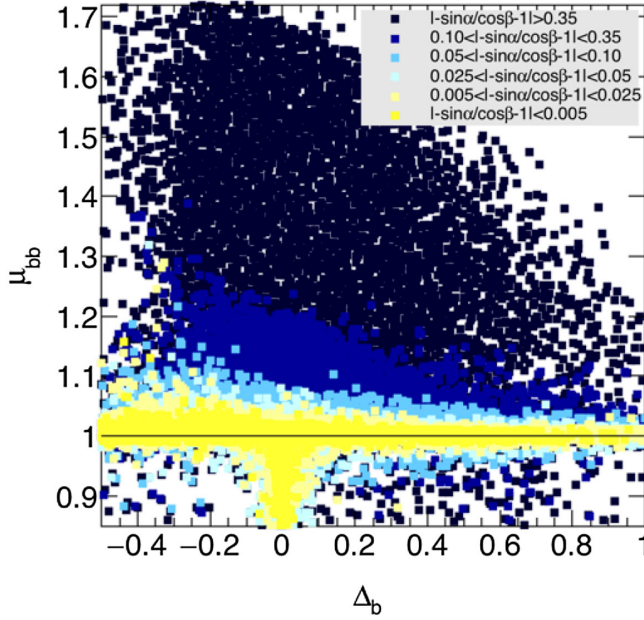
FIG. 4. $h \to b\bar{b}$ branching fraction normalized to the SM value, μ_{bb}, shown as a function of Δ_b for pMSSM points at different distances from the decoupling limit expressed by $-\sin\alpha/\cos\beta \to 1$. The convergence of μ_{bb} towards one independent of the value of Δ_b for pMSSM points approaching the decoupling limit (represented by the lighter color squares on the plot) is evident.

$\alpha \to \beta - \frac{\pi}{2}$, so that the SM–like $hb\bar{b}$ coupling is recovered: $\kappa_b \to c_b^0 \to 1$ for $M_A \gg M_Z$. The Δ_b correction is extremely important as it would significantly alter the partial width of the decay $h \to b\bar{b}$ that is by far the dominant one and, hence, affect the branching fractions of all other h decay modes in an anticorrelated way.

Similarly to the bottom quark case, a direct correction Δ_τ from stau-Higgsino loops can affect the $h\tau\tau$ vertex, shifting the coupling c_τ^0 to κ_τ as in Eq. (26), and is given in Eqs. (15) and (16). Being proportional to the electroweak coupling instead of the strong coupling, this correction is much smaller than Δ_b.

For the light scalar Higgs couplings to bottom quarks in the decoupling regime, the typical scaling of the Yukawa couplings is described by

$$\kappa_b = c_b^0 \left\{ 1 + \frac{\Delta_b}{1 + \Delta_b} \frac{2\chi}{s_{2\beta}} \right\}$$
$$= c_b^0 \left\{ 1 + \frac{\Delta_b}{1 + \Delta_b} \chi \frac{1 + \tan^2\beta}{\tan\beta} \right\}, \quad (27)$$

with χ given in Eq. (23). The corresponding scaling of the coupling factor c_b^0 has been provided in Eq. (25). For positive values of Δ_b the additional direct corrections to the bottom Yukawa coupling compensate the deviation of the indirect contributions of Eq. (25) in the decoupling limit to a large extent such that the overall deviations to the SM

limit are reduced. This is confirmed by the scan results presented in Fig. 4 that shows the signal strength μ_{bb} of the partial width $\Gamma(h \to b\bar{b})$ as a function of Δ_b for different ranges of the deviations of the tree-level-like coupling c_b^0 of Eq. (21) from the SM limit. This conclusion emerges from the additional fact that the SUSY remainder in the partial width $\Gamma(h \to b\bar{b})$ is tiny as exemplified in Ref. [38]. For small and negative values of Δ_b, the deviation of the direct corrections from the SM limit is suppressed as well, since it is proportional to $\chi\Delta_b$. This explains our findings displayed in Fig. 4. The analogous considerations are valid for the τ Yukawa coupling, too. This implies that with the present constraints on the light scalar MSSM Higgs couplings the sensitivity to Δ_b effects is suppressed so that it will not allow for a fit of $\mu \tan\beta$.

Direct corrections also affect the $ht\bar{t}$ couplings with the major difference that these are suppressed by $\tan\beta$ and hence, can be important only at very low $\tan\beta$, $\tan\beta \approx 1$. The $ht\bar{t}$ coupling is modified according to

$$\kappa_t = c_t^0 \times \frac{1 - \Delta_t \tan\alpha \tan\beta}{1 + \Delta_t}, \quad (28)$$

where Δ_t is the correction of Eq. (19). Again, in the decoupling limit, one would have $\tan\alpha \to -1/\tan\beta$ and thus, recover the SM-like coupling. However, in this case, we have ignored all these direct corrections as they turned out to be small.

In the case of the charm quark, the same direct correction holds but the term $\propto \lambda_s$ can be neglected, since the strange Yukawa coupling is negligible in all cases. The direct corrections in the case of the charm quark and the tau lepton can be neglected in general for two simple reasons. First, their impact should be smaller than in the case of the Δ_b and Δ_t corrections, and if a small deviation is observed in the two vertices, a very large distortion of the hbb or $ht\bar{t}$ vertices should be first noticed. In addition, these couplings appear only in the branching ratios for the decays $h \to c\bar{c}$ and $h \to \tau^+\tau^-$ which, as will be seen later, are rather small being below the 5% level. As the direct corrections cannot be very large (these are radiative corrections after all and should be at most at the level of 10%), they will affect the total Higgs decay width, and hence, the other Higgs branching ratios, only marginally, i.e., with deviations much below the 1% level. Hence, as their impact is far less important than the Δ_b correction, for instance, these direct corrections should be taken into account only if the branching fractions $BR(h \to c\bar{c})$ and $BR(h \to \tau^+\tau^-)$ are measured at the percent level.

Finally, we should note that because the direct corrections in the case of the $h \to WW^*$ and $h \to ZZ^*$ decays are small, one can use the approximation,

$$\kappa_V = c_V^0,$$

which is good in the most relevant cases.

III. THEORETICAL AND PARAMETRIC UNCERTAINTIES IN THE STUDY OF HIGGS PROPERTIES

We discuss now the theoretical and parametric uncertainties in the Higgs decay branching ratios and in the production cross sections.[6]

A. Theoretical and parametric uncertainties in decays

In this analysis, the light scalar Higgs boson primarily decays into bottom and to a lesser extent into charm quarks, tau leptons and gluons. Decays into four-fermion final states mediated by off shell W and Z boson pairs and into photon pairs are also considered. The corresponding uncertainties of their predictions emerge from the theoretical uncertainties due to uncalculated higher-order corrections and from the parametric uncertainties induced by the uncertainties of the input parameters, i.e., primarily the quark mass values and the strong coupling constant for fixed supersymmetric parameters.

The pure QCD corrections to the Higgs decays into quarks are known up to N^{4}LO [34] thus leaving a residual uncertainty of about 0.3% for the QCD part. On the other hand, SUSY-QCD corrections are only included up to NLO exactly [33,35] and the NNLO corrections to the dominant part Δ_b of the SUSY-QCD corrections [36–39]. This yields an estimate of up to 3%–4% residual uncertainty for the full SUSY-QCD part of these decay modes depending on the MSSM scenario. The (SUSY-)electroweak corrections are known up to NLO [32,33] but are not included in our analysis completely. Only the dominant SUSY-electroweak corrections contained in the $\Delta_{b/\tau}$ approximation are included for the Higgs decays into bottom quarks and tau leptons. This approximation generates an uncertainty of about 3%–5% for the missing electroweak effects in general. Combining all these individual uncertainties, the theoretical uncertainties for the partial widths of the decays into quarks and leptons can be estimated to be about 5%. A reduction of these uncertainties to the percent level requires, on the one hand, the complete inclusion of all known corrections and, on the other hand, the calculation of the full NNLO SUSY–QCD corrections at least. The latter step will be a task that may require a long timescale from now, since the necessary techniques for such involved NNLO calculations are

---

[6]It has been advocated that a large part of the theoretical uncertainties that affect the Higgs production rates (in particular, in the main gluon fusion mechanism) and some ambiguities that affect the branching ratios (such as the one entering in the total decay width like invisible decay channels) would cancel when measuring ratios of signal strengths for the same production process [51]. This aspect should be taken into account in the experimental analyses by the full correlation matrix of the various measurements that have been performed. We will therefore not discuss it further in this work.

TABLE I. Values of the input parameters used in this study and their uncertainties [26,54].

Parameter	Value
$\alpha_s(M_Z)$	0.1181 ± 0.0011
m_t^{pole}	(173.1 ± 0.6) GeV
$\bar{m}_b(\bar{m}_b)$	(4.18 ± 0.03) GeV
$\bar{m}_c(3\ \text{GeV})$	(0.986 ± 0.026) GeV

beyond the present state-of-the-art due to the many different masses involved in the two-loop corrections.

The (SUSY-)electroweak corrections to the Higgs decays into four fermions are known up to NLO [52,53] but are not included in our analysis. Their omission induces a theoretical uncertainty of about 5% for the decays into four fermions. The inclusion of the (SUSY-)electroweak corrections would reduce this uncertainty to the percent level. For the Higgs decay mode into two photons, the electroweak and QCD corrections are small [40,41]. The full SUSY-electroweak and SUSY-QCD corrections are still unknown. Only the pure NLO QCD corrections are included in our analysis [40]. The total theoretical uncertainty can thus be estimated to be less than 3%–5%. This uncertainty can be reduced to the percent level, once the full NLO corrections become available.

On the other hand, the parametric uncertainties induced by the input parameters, i.e., the strong coupling constant $\alpha_s(M_Z)$, the $\overline{\text{MS}}$ bottom quark mass $\bar{m}_b(\bar{m}_b)$, and the top quark mass m_t dominantly and the $\overline{\text{MS}}$ charm quark mass $\bar{m}_c(3\ \text{GeV})$ to a lesser extent are relevant. The values used in our analysis including their uncertainties are collected in Table I [26,54]. It should be noted that the $\overline{\text{MS}}$ mass values for the bottom and charm quarks develop a correlation with the value of the strong coupling constant $\alpha_s(M_Z)$ that can be neglected [54]. Future developments on the lattice may reduce the hadronic parameter uncertainties, i.e., the ones of the bottom and charm masses and of the strong coupling constant α_s, significantly within the next 10 years, i.e., by factors of 2–5 typically.

The corresponding analysis [55,56] for the SM Higgs boson leads to total uncertainties of the branching ratios of about 2% for $H \to b\bar{b}, \tau^+\tau^-$, 7% for $H \to c\bar{c}$, 3% for $H \to \gamma\gamma$, and 2% for $H \to WW, ZZ$ by using the updated values of Table I for the input parameters. These uncertainties correspond to the same uncertainties for the branching ratios of the light MSSM Higgs boson in the decoupling limit of large pseudoscalar masses M_A, where it becomes SM-like, since then also the dominant SUSY effects emerging from the $\Delta_{b/\tau}$ corrections to the b/τ Yukawa coupling vanish. Away from this decoupling limit the total uncertainties become larger due to the larger uncertainties induced by the genuine SUSY-QCD and -electroweak corrections. For the heavy Higgs bosons, the additional uncertainties related to these SUSY-specific

corrections have to be included in all accessible scenarios thus adding another 3%–5% to the total uncertainty depending on the MSSM scenario, while for the light Higgs these corrections are suppressed in most cases.

B. Theoretical and parametric uncertainties in Higgs production

1. QCD uncertainties

The main SM-Higgs production channel is the top- and bottom-loop mediated gluon-fusion mechanism and, at $\sqrt{s} = 7$–14 TeV, the three other mechanisms contribute at a level below 15% within the SM when their rates are added and before kinematical cuts are applied. The majority of the signal events presently observed at the LHC, in particular in the main search channels $h \to \gamma\gamma$, $h \to ZZ^* \to 4\ell$, $h \to WW^* \to 2\ell2\nu$ and, to a lesser extent, $h \to \tau\tau$, thus originate from the gluon-fusion mechanism, which is significantly affected by theoretical uncertainties. Even the VBF channel, for which the theoretical uncertainty is smaller when the inclusive cross section is considered, is contaminated by the gluon-fusion channel and the uncertainties become relevant once kinematical cuts are applied. The impact of these theoretical uncertainties is summarized below.

Until quite recently, the inclusive cross section for the process $gg \to h$ has been known up to next–to–next–to–leading order (NNLO) in the heavy-top limit (HTL) in perturbative QCD [57,58], increasing the cross section at $\sqrt{s} = 14$ TeV by a factor of ≈ 2 compared to the leading-order (LO) approximation and resulting in a residual scale uncertainty of $\Delta_\mu \approx \pm 8\%$ when the central values of the renormalization and factorization scales are taken to be at half of the Higgs mass, $\mu_R = \mu_F = \frac{1}{2}M_h$, and varied within a factor of 2 from this central value, $[\frac{1}{4}M_h, M_h]$. This is the scale uncertainty that has been assumed by the ATLAS and CMS Collaborations in the signal strengths from the dominant gluon-fusion channel. However, the "tour de force" of deriving $\sigma(gg \to h)$ at next-to-next–to–next–to–leading order (N^{3}LO) has been achieved recently in the HTL [59]. The new corrections increase the NNLO result of the total cross section slightly by 2% for $M_h = 125$ GeV at $\sqrt{s} = 14$ TeV for $\mu_R = \mu_F = \frac{1}{2}M_h$ and the residual scale dependence is drastically reduced from 8% to $\Delta_\mu^{\mathrm{ggh}} = +0.2\%, -2.4\%$ at N^{3}LO when the two scales are varied in the adopted range $[\frac{1}{4}M_h, M_h]$. This accuracy is underlined by the small effect of soft-gluon resummation beyond N^{3}LO [60].

Nevertheless, the calculation has some drawbacks. As the partonic cross section at N^{3}LO has been inconsistently folded with the parton distribution functions (PDFs) at NNLO, while the calculation has not yet been performed at the required order for the latter, the impact of this inconsistency has been estimated at the percent level [56].

The dominant effect is induced by the uncertainties originating from the PDF fits inherently. Indeed, as the $gg \to h$ process is of $\mathcal{O}(\alpha_s^2)$ already at leading order and is initiated by gluons, there are sizeable uncertainties due to the gluon parton distribution function and the value of the α_s coupling which when combined give at 68% confidence level (CL), $\Delta_{\mathrm{PDF}+\alpha_s}^{\mathrm{ggh}} = \pm 3.2\%$ for $M_h = 125$ GeV at $\sqrt{s} = 14$ TeV [56].

In addition, there is another source of theoretical uncertainties originating from the use of an effective field theory (EFT) approach to calculate the radiative corrections beyond the NLO approximation [57], NNLO, and N^{3}LO in QCD [58,59,61] and NNLO for the mixed electroweak–QCD corrections [62]. In both cases, only the top-quark loop in the large top-quark mass limit has been considered beyond NLO and the corrections to the b–quark loop (which gives a contribution of approximately 5% to the process at NLO [57]) which cannot be obtained in the EFT approach have been included at NLO only. However, the calculation at NLO that has been done keeping the exact quark mass dependence, has shown that the QCD corrections are significantly smaller if expressed in terms of the pole quark masses. The uncertainty of using the EFT approach beyond NLO has been estimated to be at the level of 2% [56]. This uncertainty will be slightly reduced due to the recent calculation of the full top-mass effects at NNLO [61] that turn out to be small. The total uncertainties on the inclusive cross section have been estimated as $\Delta_{\mathrm{ggh}} \approx \pm 4.5\%$ [56] that we will adopt here.[7]

In addition, significant uncertainties arise when the $gg \to h$ cross section is broken into the jet categories $h + 0j$, $h + 1j$ and $h + 2j$, as is experimentally done in order to enhance the search sensitivities in some important channels, such as $h \to WW^*$ and $h \to \tau\tau$. Indeed for these noninclusive observables the QCD corrections are known at next-to–leading order and beyond in most cases and generate large logarithms that lead to a large residual scale variation of the cross sections as well as a strong dependence on the jet cuts [64]. This problem has partly been overcome by including resummation of soft-gluon effects [56].

These kinds of uncertainties will also affect the other production processes. The VBF channel, providing the dominant contribution to the $qq \to hqq$ final state, for which the inclusive cross section is known up to N^{3}LO [65,66] in QCD and up to NLO-electroweak [67], has only a few percent combined scale and PDF uncertainty according to Ref. [56] and develops a total theoretical uncertainty of $\Delta_{\mu+\mathrm{PDF}}^{\mathrm{VBF}} \approx \pm 2.5\%$ for $M_h = 125$ GeV at $\sqrt{s} = 14$ TeV. The contamination by the gluon-fusion

---

[7]Note that other, less optimistic, estimates of these uncertainties have been made [63], but we will follow the official recommendations by the LHC Higgs Working Group.

process $gg \to h + 2j$, which leads to the same final state (and which is known at NLO in the HTL [68]) makes the total uncertainty in the $h + 2j$ final "VBF" sample a bit larger. It is included in the uncertainty estimate above.

The situation is similar for the Higgs–strahlung process where for the inclusive total cross sections, also known at NNLO QCD [69,70] and NLO electroweak [71], the total uncertainty is at the level of a few percent, $\Delta_{\mu+\text{PDF}}^{Wh} = \pm 2.5\%$ and $\Delta_{\mu+\text{PDF}}^{Zh} = \pm 5\%$ for $M_h = 125$ GeV at $\sqrt{s} = 14$ TeV [56] (in the latter case, there is an additional contribution from the $gg \to Zh$ process which is known at NLO in the HTL [72] and introduces an extra scale and PDF uncertainty so that the total uncertainty is larger than for the Wh case). Finally, the associated $pp \to t\bar{t}h$ process is known at NLO QCD [73] and NLO electroweak [74] supplemented by soft and collinear gluon resummation up to NNLL [75]. The total uncertainty is estimated to be $\Delta_{\mu+\text{PDF}}^{\text{tth}} = +9.5\%, -12.7\%$ [56] for $M_h = 125$ GeV at $\sqrt{s} = 14$ TeV. In both cases, Higgs-strahlung and $t\bar{t}h$ production, if boosted topologies are selected, the uncertainties of these exclusive rates might be considerably larger.

Within the MSSM the associated Higgs boson production with a $b\bar{b}$ pair is dominant for large values of $\tan\beta$. The QCD corrections to the inclusive cross section evaluated in the four-flavor scheme (4FS) are large [76], while within the five-flavor scheme (5FS) they are of more moderate size [77]. The reasons for this difference are the massless and on shell treatment of the bottom quarks within the 5FS and the nonresummation of PDF-related logarithms in the 4FS. Both calculations differ by about 20% and a combination is desirable. This has been solved quite recently by proper matchings between both schemes [78]. The residual uncertainties of the inclusive cross sections range at the level of about 20% [56].

In summary, the cross sections for the various channels are presently known at the level of

$$\Delta_{\text{ggh}} \approx 4.5\%, \qquad \Delta_{\text{VBF}} \approx \Delta_{\text{WH}} \approx 2.5\%,$$
$$\Delta_{\text{ZH}} \approx 5\%, \qquad \Delta_{\text{tth}} \approx 10\%, \qquad \Delta_{\text{b\bar{b}h}} \approx 20\%, \qquad (29)$$

in the SM limit which are the numbers that we will adopt in our analysis for illustration for the QCD-initiated uncertainties. It is clear that this knowledge will improve and at the time of the high-luminosity LHC option, the uncertainties could be reduced. It should be noted that these uncertainties have to be extended by the genuine SUSY uncertainties to which we turn now.

2. Genuine SUSY uncertainties

Genuine SUSY–QCD corrections are also known for the gluon-fusion processes $gg \to h/H/A$ [79,80]. They are sizeable for small values of $\tan\beta$ where the top loops provide the dominant contribution. However, at large $\tan\beta$ values, the SUSY–QCD corrections are large since the Δ_b contributions are sizeable and dominant [80]. If the leading Δ_b contributions are absorbed in the effective bottom Yukawa couplings as outlined in Sec. II E, the remainder of these contributions is of moderate size [80]. Since this contribution is not included in our analysis it has to be treated as an additional uncertainty. Using the conventions of Sec. II E, this can be estimated as $\Delta_{\text{SUSY}}^{\text{ggh}} \approx \delta\sigma\{g_t, \tilde{g}_b[\Delta_b(1 \pm 5\%)]\}/\sigma\{g_t, \tilde{g}_b\}$, if the Δ_b-resummed bottom Yukawa couplings of Eq. (17) are used for the bottom contributions. This notation is meant as a variation of the pure Δ_b terms inside the cross section prediction by 5% and taking the impact on the cross section as the uncertainty related to SUSY effects.

The genuine SUSY corrections to the VBF and Higgs-strahlung processes are small [81,82]. Only in very exceptional regions of the MSSM parameter space they can reach the 10% level. The QCD corrections are easy to include in the analysis [81]. The residual uncertainties can be estimated at the subpercent level on top of the pure QCD corrections.

The genuine SUSY–QCD corrections to the $t\bar{t}\phi$ cross sections, with $\phi = h, H, A$, are known to be of moderate size [83] on top of the pure QCD corrections. The residual uncertainties induced by these corrections can be estimated to about 5% conservatively. On the other hand, the genuine SUSY-QCD corrections to $b\bar{b}\phi^0$ production can be absorbed in the resummed bottom Yukawa couplings of Eq. (17). The remainder beyond this approximation is small, i.e., of subpercent level [83,84]. The resummed bottom Yukawa coupling of Eq. (17) includes, in our study, SUSY–electroweak corrections.

IV. ANALYSIS

In order to relate the measurements of the Higgs properties at the LHC and an e^+e^- collider to the fundamental SUSY parameters, it is necessary to choose an explicit model. In this study, we adopt the pMSSM, a generic implementation of the MSSM with the neutralino being the LSP, having all the soft SUSY-breaking mass terms and trilinear couplings as free parameters.

A. Scans in the pMSSM

We vary the 19 pMSSM free parameters in an uncorrelated way through flat scans within the ranges given in Table II. The scan range is explicitly chosen to include the so-called "maximal mixing" region [16], at $X_t \sim \sqrt{6}M_{\text{SUSY}}$, which corresponds to the larger values of M_h achievable in the MSSM, and to reach SUSY masses beyond the reach of direct SUSY searches at the LHC. The details of the pMSSM scans and the tools used for the computations of the spectra and relevant observables have been presented elsewhere [85]. Here, we mention only those most relevant to this study. SUSY mass spectra are generated with

TABLE II. pMSSM parameter ranges adopted in the scans (in GeV when applicable).

Parameter	Range
$\tan\beta$	[1, 60]
M_A	[50, 6000]
M_1	[−5000, 6000]
M_2	[−5000, 6000]
M_3	[50, 6000]
$A_d = A_s = A_b$	[−10000, 10000]
$A_u = A_c = A_t$	[−10000, 10000]
$A_e = A_\mu = A_\tau$	[−10000, 10000]
μ	[−6000, 6000]
$M_{\tilde{e}_L} = M_{\tilde{\mu}_L}$	[50, 6000]
$M_{\tilde{e}_R} = M_{\tilde{\mu}_R}$	[50, 6000]
$M_{\tilde{\tau}_L}$	[50, 6000]
$M_{\tilde{\tau}_R}$	[50, 6000]
$M_{\tilde{q}_{1L}} = M_{\tilde{q}_{2L}}$	[50, 6000]
$M_{\tilde{q}_{3L}}$	[50, 6000]
$M_{\tilde{u}_R} = M_{\tilde{c}_R}$	[50, 6000]
$M_{\tilde{t}_R}$	[50, 6000]
$M_{\tilde{d}_R} = M_{\tilde{s}_R}$	[50, 6000]
$M_{\tilde{b}_R}$	[50, 6000]

TABLE III. Summary of the flavor physics constraints applied to the accepted points in the pMSSM scans. The range for $B_s \to \mu\mu$ is based on the average reported in Ref. [98] obtained with the technique developed by the ATLAS, CMS, and LHCb Collaborations [99].

Constraint	Value	References
$b \to s\gamma$	$3.05 < BR < 3.59 \ (\times 10^{-4})$	[97]
$B \to \tau\nu$	$0.71 < BR < 1.47 \ (\times 10^{-4})$	[26]
$B_s \to \mu\mu$	$2.10 < BR < 3.60 \ (\times 10^{-9})$	[93–95]

SOFTSUSY 3.2.3 [86], which gives results that are comparable to other spectrum generators such as Suspect [87]. As already mentioned, the decay branching fractions of Higgs bosons are obtained using HDECAY 6.53 [23], including gaugino and sfermion loop corrections, and cross-checked with FeynHiggs 2.8.5 [88]. The widths and decay branching fractions of the other SUSY particles are computed using SDECAY 1.3 [89]. The flavor observables and dark matter relic density are calculated with the programs SuperIso Relic v3.2 [90] and micrOMEGAs [91].

As for the Higgs production rates, the gg and bb production cross sections are computed using HIGLU 1.2 [92] and FeynHiggs 2.8.5 [88], respectively. The Higgs production cross sections and the branching fractions for decays into $\gamma\gamma$ and WW, ZZ from HIGLU and HDECAY are compared to those predicted by FeynHiggs.

In the SM, both the $gg \to H_{SM}$ cross section and the branching fractions agree within ∼3%. Significant differences are observed in the SUSY case, with HDECAY giving values of the branching fractions to $\gamma\gamma$ and WW that are on average 9% lower and 19% larger, respectively, than those predicted by FeynHiggs and have a root mean square (rms) spread of the distribution of the relative difference between the two programs of 18% and 24%, respectively. In this study, we adopt the HDECAY results throughout the analysis. The parametric uncertainties have been discussed in Sec. III.

The SM $\gamma\gamma$, WW and ZZ branching fractions receive electroweak corrections, of the order of 5%–10%, which are included in HDECAY. However, their SUSY counterparts are not known. In order to make the SM and SUSY branching fractions comparable in this study, we remove the electroweak corrections to their SM values.

The "valid" pMSSM points are selected by requiring the neutralino to be the LSP and the lightest Higgs boson mass to be in the range $122 < M_h < 128$ GeV. These requirements reduce the sample to ≃1.7 M points. In addition, we impose a set of constraints from flavor physics and relic dark matter data, as discussed in [85], to obtain a set of "accepted" pMSSM points used in the subsequent analysis. The main flavor physics measurements, summarized in Table III, are the decay $B_s \to \mu^+\mu^-$ [93–95], that can receive important SUSY contributions at large values of $\tan\beta$ [96], the inclusive rare decay $B \to X_s\gamma$ [97], and the leptonic decay $B \to \tau\nu_\tau$ [26].

The relic DM density constraint is applied in a loose form, requiring the contribution by the $\tilde{\chi}$ LSP, Ω_χ, not to exceed the upper limit of the Ω_{CDM} density determined by the PLANCK satellite [100], i.e., $10^{-5} < \Omega_\chi h^2 < 0.163$, thus allowing for other particles to contribute to the observed cosmic DM and/or modifications to the early universe properties.

The last decade has been rich in results from experiments searching for the scattering of WIMPs on solid state and gaseous detectors located in underground laboratories. Currently, the results from the XENON 1T [101] stand as the most constraining bounds on the WIMP scattering cross section as a function of its mass. The use of these bounds in the analysis of the pMSSM scan points brings a considerable dependence on the assumptions on the dark matter profile in our Galaxy. While we do not use these bounds in the preselection of the accepted pMSSM points, we do discuss their impact, as well as that of the next generation of direct dark matter detection experiments, on the pMSSM parameter space in relation to the Higgs invisible decay rate.

After applying these constraints, the pMSSM scans yield ≃0.8 M accepted points. The results discussed in Sec. V depend on the distributions of MSSM variables for the valid and accepted points. Although the pMSSM scans are flat in
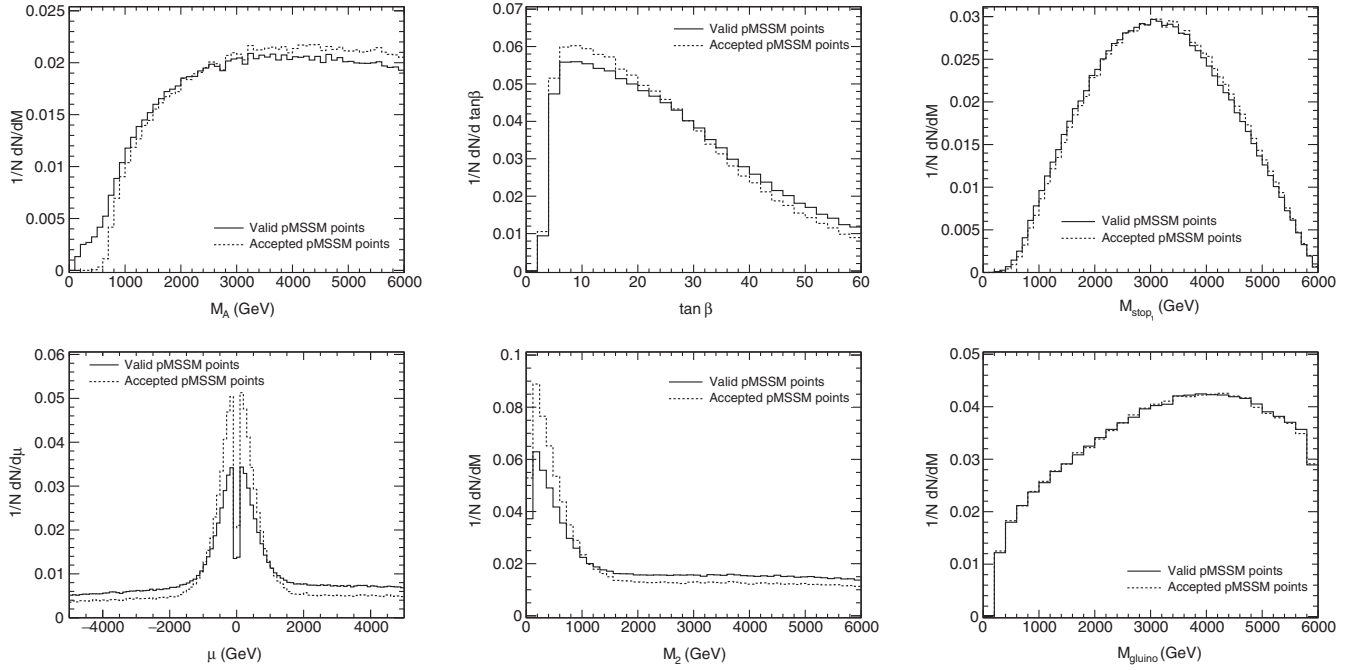
FIG. 5.   Distributions of the M_A (upper left), $\tan\beta$ (upper center), $M_{\tilde{t}_1}$ (upper right), μ (lower left), M_2 (lower center), $M_{\tilde{g}}$ (lower right panel) pMSSM parameters of valid (continuous line), and accepted (dashed line) points. The shapes of these distributions depend both on the range of the pMSSM parameters adopted in the scans (see Table II) and on the requirements for valid and accepted scan points.

the input variables according to the ranges given in Table II, the distributions of these variables for the valid and accepted points are characterized by a nonflat rate of points across the range of each variable. This is an effect of the selection based on M_h, flavor observables and dark matter relic density. The distribution of the pMSSM parameters most relevant to this study for the valid and the accepted scan points are given in Fig. 5.

B. SUSY particle direct searches at the LHC

The ATLAS and CMS experiments at the LHC have pursued a vast program of searches for SUSY particles. These cover both the production of particles cascading to quarks and/or leptons and the neutralino LSP, through channels with jets and/or leptons + MET, and that of the heavy SUSY Higgs bosons, H, A, and $H^\pm$.

In this study, we test the compatibility of the accepted pMSSM points with the bounds implied by the LHC searches. We consider the bounds obtained from the analyses given in Table IV. These can be divided in four classes: (i) $H/A \to \tau\tau$, ZZ and $t\bar{t}$ decays; (ii) channels with jets $(+\ell)$ + MET, sensitive to gluino and scalar quark production and decays, (iii) channels with ℓs $(+h)$ + MET sensitive to chargino and neutralino production and decays, and (iv) monojets + MET sensitive to production of $\tilde{\chi}\tilde{\chi}$ or $\tilde{q}\tilde{q}$, where the scalar quark is highly degenerate with the neutralino LSP. While there is an impressively large number of final states considered by the experiments, the chosen analyses provide an efficient coverage of the

MSSM parameter space within a practical number of processes to be simulated and reconstructed for each pMSSM point. Events are generated with `MadGraph 5` [102] and `Pythia 8.2` [103]. Physics observables are obtained through a parametric simulation for the detector response and event reconstruction using `Delphes 3.4` [104] fast simulation. Signal selection cuts for each of the analyses are applied to the simulated signal events. The number of SM background events in the signal regions are

TABLE IV.   Summary of the analyses used to assess the observability of the pMSSM points by the LHC SUSY searches.

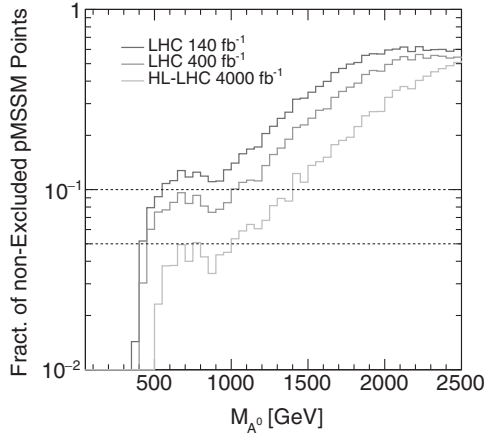| Channel	Integrated luminosity fb^{-1}	Sensitivity	References
$H/A \to \tau\tau$	36	H, A	[106]
$H/A \to ZZ$	36	H, A	[107]
$H/A \to t\bar{t}$	20	H, A	[108]
jets + MET	139	$\tilde{g}$, $\tilde{q}$	[109]
jets + MET	36	$\tilde{g}$, $\tilde{q}$	[110]
1ℓ + jets + MET	36	$\tilde{g}$, $\tilde{q}$	[111]
$\ell^+\ell^+$, $\ell^-\ell^-$ + MET	139	$\tilde{g}$, $\tilde{q}$	[112]
b jets + MET	36	$\tilde{t}$	[113]
multiple b jets + MET	80	$\tilde{t}$, b	[114]
2ℓ + MET	139	$\tilde{\chi}^0$, $\tilde{\chi}^\pm$, $\tilde{\ell}$	[115]
3ℓ + MET	36	$\tilde{\chi}^0$ $\tilde{\chi}^\pm$, $\tilde{\ell}$	[116]
monojet + MET	36	$\tilde{\chi}\tilde{\chi}$, $\tilde{q}\tilde{q}$	[117]
mono-W/Z + MET	3.2	$\tilde{\chi}\tilde{\chi}$, $\tilde{q}\tilde{q}$	[118]

FIG. 6.   Fraction of accepted pMSSM points not excluded at 95% CL by the present H/A searches and beyond the expected sensitivity of run 3 and HL-LHC as a function of M_A.

taken from those estimated by ATLAS for the analyses listed in Table IV. The 95% CL exclusion of each SUSY point in presence of background only is determined using the CLs method [105].

Results from the present run 2 analyses are projected to the integrated luminosities reachable after run 3 and HL-LHC operation by rescaling the signal and background event yields. Accepted pMSSM scan points yielding a rate of SUSY events incompatible with the background-only hypothesis using the CLs method for a given integrated luminosity are considered as "excluded" at the corresponding stage of the LHC program. The other pMSSM points are considered as "not excluded".

The fraction of accepted pMSSM points not excluded by the present searches and beyond the sensitivity of run 3 and the HL-LHC are shown in Fig. 6 for the H/A search channels as a function of M_A and in Fig. 7 for the jet/ℓ + MET searches as a function of the $\tilde{t}_1$, $\tilde{g}$, and $\tilde{\chi}_1^0$ masses.

In particular, the M_A values at which more than 90% of the accepted pMSSM points are excluded by the H/A searches at 95% CL are ~500 GeV for the present run 2 ATLAS data, 1000 GeV for the run 3, and 1400 GeV for the HL-LHC statistics. The fraction of pMSSM points excluded by the $H/A \to \tau\tau$ and the jets and leptons + MET searches are summarized in Table V. The jet/ℓ + MET searches have already excluded more than 90% of the accepted pMSSM points up to a gluino mass of 1400 GeV, a lighter scalar top mass of 400 GeV, and a lightest chargino mass of 200 GeV, with an expected sensitivity extending to 2000, 1200, and 500 GeV, respectively, by the end of the HL-LHC program.

C. Higgs measurement accuracy at the LHC and e^+e^- colliders

The measurements of the Higgs properties provide at least two sets of constraints on the MSSM. First, the prediction of
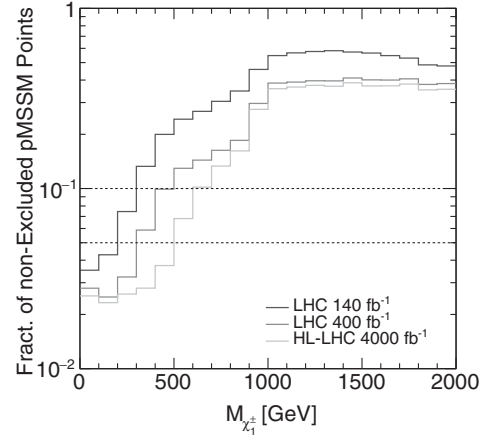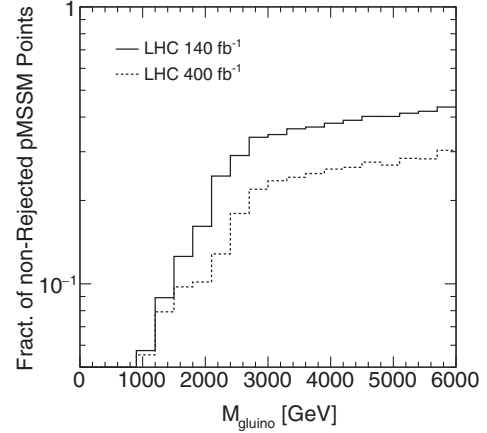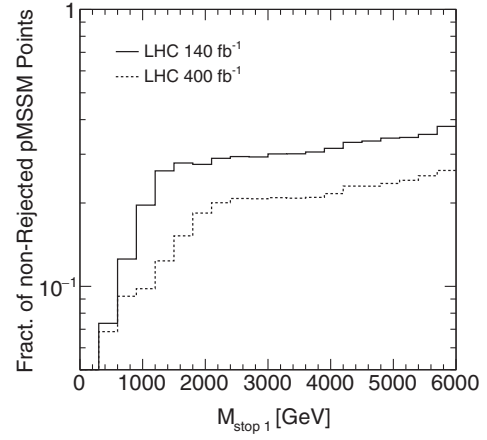

FIG. 7.   Fraction of accepted pMSSM points not excluded at 95% CL by the present jet/ℓ + MET searches and beyond the expected sensitivity of run 3 and HL-LHC as a function of the scalar top (top panel), gluino (center panel), and lightest chargino (bottom panel) masses.

the M_h value in SUSY provides a constraint on the parameters when the measured value is imposed. Given the measured value of 125 GeV, the MSSM parameters need to be properly chosen to reach this mass, for example, by selecting the so-called "maximal mixing" solutions. While imposing the constraint 122 GeV < M_h < 128 GeV keeps

TABLE V. Fractions of accepted pMSSM points excluded by the LHC $H/A \to \tau\tau$, ZZ, $t\bar{t}$, and the jet/ℓ + MET searches at three stages of the LHC program.

	LHC	LHC	HL-LHC
	140 fb^{-1}	400 fb^{-1}	4 ab^{-1}
$H/A \to \tau\tau$, ZZ, $t\bar{t}$	0.10	0.12	0.19
+j/ℓs + MET	0.47	0.52	0.65

only ~10% of the accepted pMSSM points, the M_h value *per se* does not provide any discrimination between SM and SUSY Higgs. Then, the Higgs decay yields in the accessible final states provide us with an opportunity to further constrain the MSSM parameter space and possibly tell a SUSY Higgs from the SM boson.

In this study, we consider the values of the coupling modifiers, κ_X, obtained by ATLAS combining the present analyses of run 2 data with luminosities up to 139 fb^{-1} [119] given in Table VI and the HL-LHC program [120] given in Table VII. The accuracies for the determination of the Higgs couplings at future e^+e^- Higgs factories are taken from the compilation in [121] and given in Table VII.

For each accepted pMSSM point, the values of the coupling modifiers, κ_X, for the accessible channels are

TABLE VI. Best fit values for the Higgs boson coupling modifiers κ_X from the combination of the ATLAS measurements, with effective photon and gluon couplings under the assumption that the SM decay channel saturates the Higgs decay width [119].

	13 TeV
Channel	25–79.8 fb^{-1}
κ_W	1.06 ± 0.06
κ_Z	0.99 ± 0.06
κ_t	0.92 ± 0.10
κ_b	0.87 ± 0.11
κ_τ	0.92 ± 0.07
κ_γ	1.04 ± 0.06
κ_g	$0.92^{+0.07}_{-0.06}$

computed using HDECAY. The compatibility of the pMSSM with the LHC measurements is determined by computing the χ^2 value as $\chi^2 = x^T M^{-1} x$, where x is the vector, of size N, of the differences between the values of the coupling modifiers predicted for the pMSSM point x_{pMSSM} and those measured by the experiment x_{exp} (or the SM predictions for the future results) and M is the $N \times N$ covariance matrix of the measurement, including correlations, reported by the experiment [119]. This expression extends the χ^2 definition to a set of N correlated variables. The compatibility of each pMSSM point is determined at a given CL from the χ^2 probability $\mathrm{Prob}(\chi^2, N)$, where the number of degrees of freedom corresponds to the number of observables, N. For the present results of Ref. [119], the fitted values are used as central values x_{exp}, while for the projected performance at run 3 and HL-LHC the x_{exp} are taken to be the SM values and the correlation matrix is assumed to be the same as that of the current combination [119].

At an e^+e^- collider, the $e^+e^- \to Zh \to \ell\ell X$ process is available for a model-independent determination of the production cross section from the recoil mass of the $\ell\ell$ system and the branching fraction can be directly measured [122]. The accuracy in the determination of the Higgs decay branching fractions and couplings have been studied in great details first for an e^+e^- linear collider at $\sqrt{s} = 250 - 500$ GeV [123,124] and, more recently, extended to higher center-of-mass energies. Results obtained first with fast simulation have been confirmed by subsequent studies based on detailed GEANT-4 full simulation and reconstruction with the inclusion of (at least some of) the beam-induced backgrounds. Detector R&D has also greatly progressed towards a validation of the unprecedented response performances assumed in the ILC studies. An important outcome of the studies of e^+e^- collisions at energies above 500 GeV has been the indications of significant improvements in the determination of the Higgs properties through the $e^+e^- \to WW\nu\nu \to h\nu\nu$ fusion process, whose cross section increases $\propto \log\frac{s}{M_h^2}$ and exceeds the peak value of the $e^+e^- \to hZ$ Higgs-strahlung cross section for $\sqrt{s}$ energies ≥ 480 GeV.

TABLE VII. Assumed accuracies on the h boson coupling modifiers κ_i for future collider projects (from Ref. [121]).

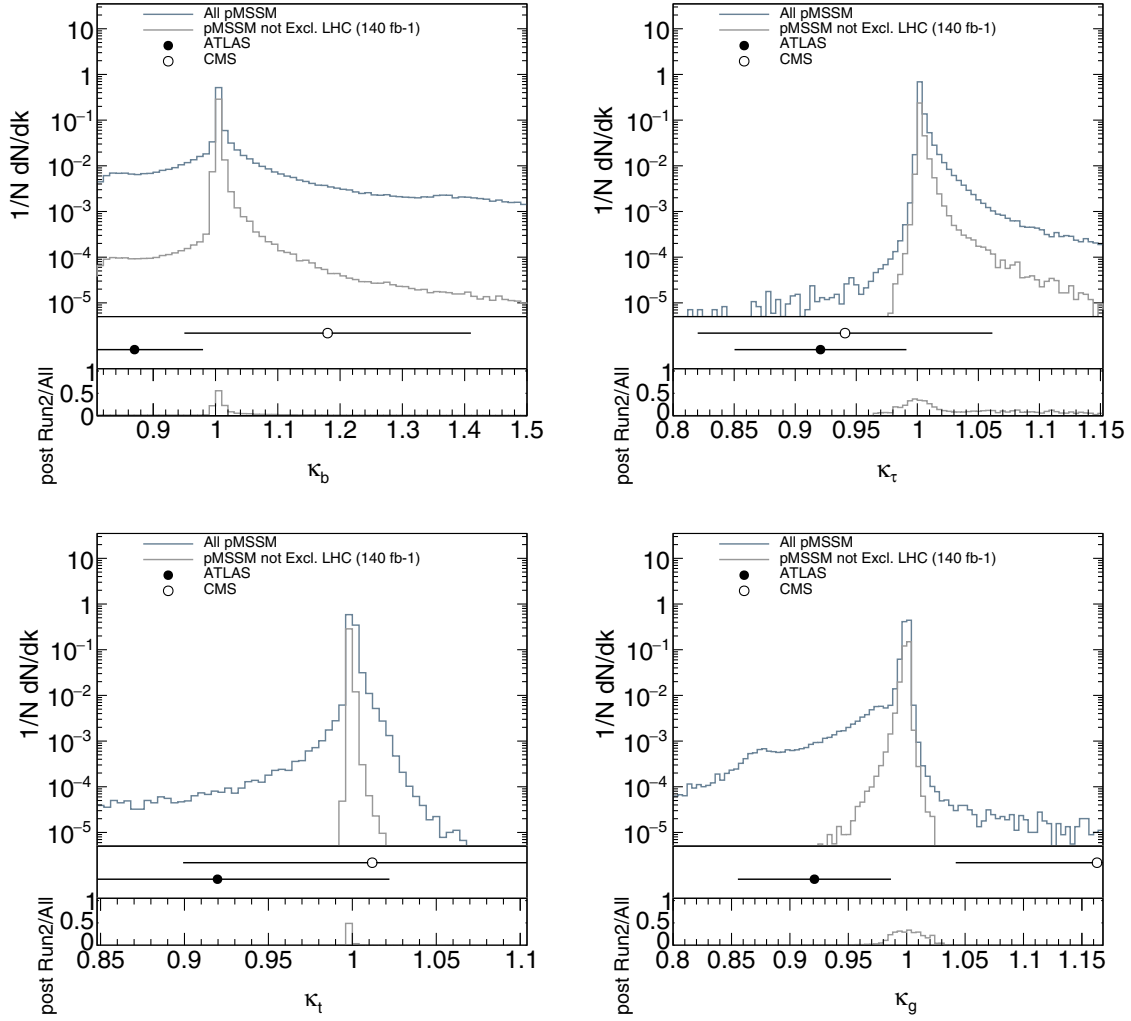|		ILC	ILC	ILC	FCC-ee	FCC-ee
Channel	HL-LHC	250 GeV	500 GeV	1 TeV	240 GeV	365 GeV
κ_W	0.017	0.0180	0.0029	0.0024	0.013	0.0043
κ_Z	0.015	0.0029	0.0023	0.0022	0.0020	0.0017
κ_t	0.033	$\cdots$	0.0690	0.016	$\cdots$	$\cdots$
κ_b	0.036	0.0180	0.0058	0.0048	0.0130	0.0067
κ_c	$\cdots$	0.025	0.0130	0.0090	0.018	0.013
κ_τ	0.019	0.0190	0.0070	0.0057	0.0140	0.0073
κ_γ	0.019	0.0670	0.034	0.019	0.047	0.039
κ_g	0.023	0.0230	0.0097	0.0066	0.0170	0.0100

FIG. 8. h Higgs boson coupling modifiers, κ_X, to b quarks (upper left), τ leptons (upper right), top quarks (lower left) and gluons (lower right) for all valid pMSSM points and those not excluded by the LHC run 2 searches compared to the present measurements by the ATLAS [119] and CMS [125] experiments. The lower panels show the fractions of nonexcluded pMSSM points as a function of κ_X.

V. RESULTS

In this section, we analyze the potential of measurements of the Higgs boson effective couplings at the LHC and future colliders, discussed in the previous sections, to exclude, or identify, MSSM solutions in the parameter space of the pMSSM not excluded by direct searches for heavy Higgs bosons and for SUSY particles in channels with missing E_T signatures. The analysis uses as inputs the coupling modifier terms, κ_X, obtained in the context of the so-called κ framework, discussed in Sec. III, by assuming the central values and uncertainties summarized in Sec. IV C.

First, we compare the distributions of these coupling modifiers predicted for the valid pMSSM points in our scans to those obtained for the points not excluded by the direct searches in run 2 and to the current measurements (see Fig. 8). It is also instructive to compare the coupling

modifier values, κ_X, for the pMSSM points to those obtained so far for the LHC data by correlating particles as shown in Fig. 9.

In all these comparisons, the current experimental accuracy is close to the full spread of the pMSSM predictions. In this sense, the statement that the properties of the observed Higgs boson are SM-like could also be rephrased by saying that they are also MSSM-like. However, a fraction of the pMSSM solutions is found to be incompatible with these measurements, and more will be tested at the HL-LHC and later by a possible e^+e^- Higgs factory. It is interesting to understand the Higgs coupling properties of the points that are preferentially discarded by direct searches. Comparing the κ_X distributions for all the valid pMSSM points to those for the points not excluded by the direct LHC searches for heavy Higgs bosons and those for SUSY particles in missing E_T channels, it is evident that these preferentially excluded pMSSM points are located on
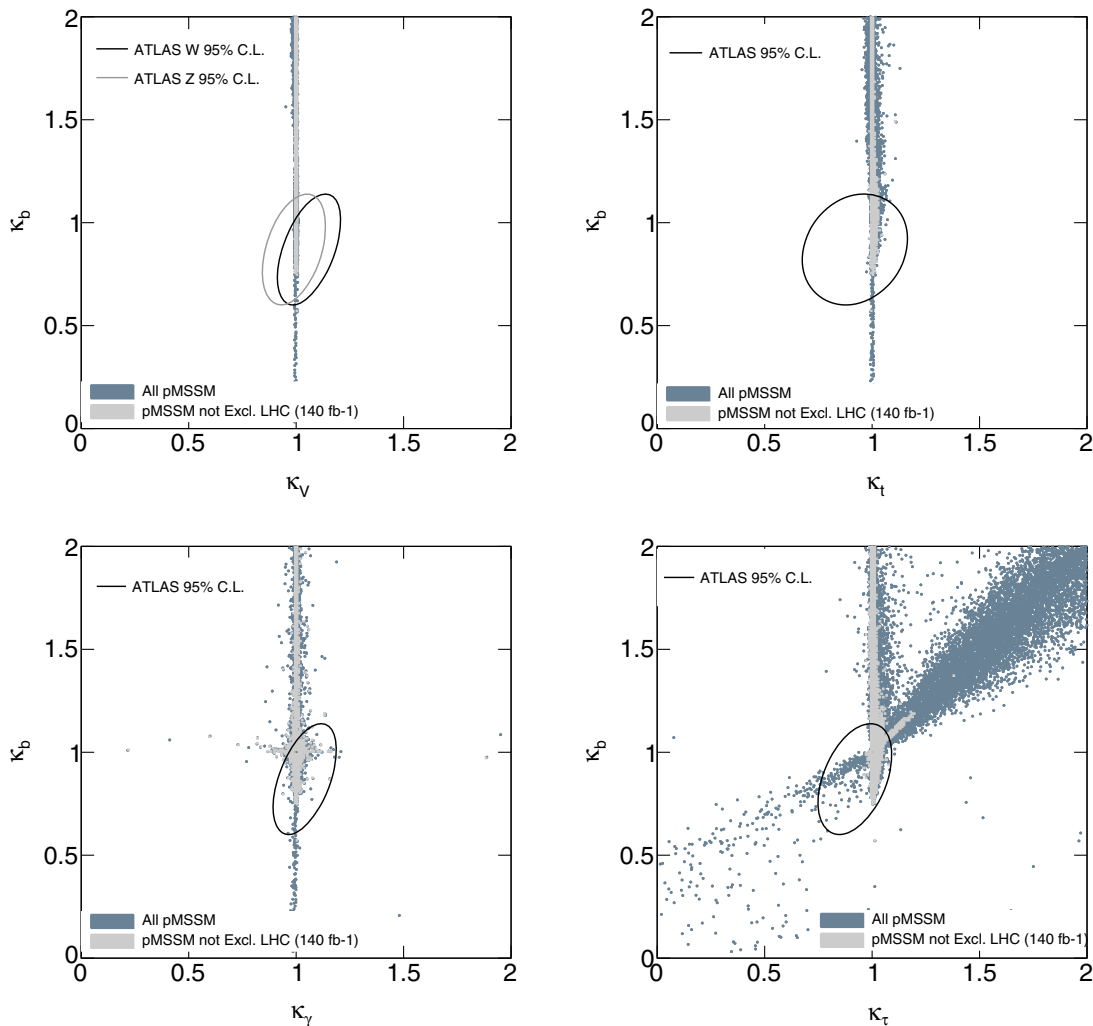
FIG. 9.   Correlations of the h Higgs boson κ coupling modifiers comparing the valid pMSSM points, those not excluded by the LHC run 2 searches and the 95% CL contours of the current measurements by the ATLAS experiment [119].

the tails of k_i distributions at values away from the SM predictions, corresponding to $\kappa_X = 1$. The large reduction of pMSSM points at κ values significantly above the SM expectations for the b quarks and τ leptons induced by the SUSY searches is mostly due to the constraint on M_A set by the searches in the $H/A \rightarrow \tau^+\tau^-$ channel.

These effects are discussed in quantitative terms in the next section. This is done by studying the fractions of valid and accepted pMSSM points that can be excluded by the Higgs coupling measurements with the accuracies expected for the next steps of the LHC program and for future colliders in relation to their observability at the LHC in new particle searches. In addition, the constraints that can be derived from these measurements on the relevant MSSM parameters are discussed.

A. Constraints on the pMSSM

The compatibility of the Higgs couplings with the predictions for the SM or for specific MSSM scenarios

defines a way to study the sensitivity for identifying SUSY and discriminate between different scenarios as a function of the collider data accuracy in the light Higgs couplings. Since increasing the integrated luminosity increases the precision of the Higgs property measurements as well as the mass bounds from direct searches, if no signal is observed, this study estimates also the complementarity between the direct (jets/ℓs + MET and heavy Higgs bosons) and indirect (Higgs properties) probes of new physics in the context of SUSY. In particular, we study how the indirect sensitivity evolves with increasing the accuracy of the Higgs measurements and determine the expected impact of the improved accuracy from an e^+e^- Higgs factory, given the current reach of the SUSY searches by the LHC experiments.

The test is performed by computing the χ^2 probability of the Higgs observables for each pMSSM point with respect to the actual measurements or the SM hypothesis and measuring the fraction of accepted pMSSM points incompatible with the SM at the 90% CL. This is the fraction of

TABLE VIII. Fraction of pMSSM points excluded at 90% CL by the Higgs coupling measurements with the LHC run 2 and the estimated HL-LHC accuracies. The first lines of each block gives the fractions for all valid and accepted pMSSM points, the following row the fractions of the pMSSM points excluded only by Higgs couplings and not by the searches for H/A heavy Higgs bosons and those in the jets and/or leptons + MET channels with the run 2 and the HL-LHC sensitivity.

pMSSM	LHC	HL-LHC
Selection	140 fb^{-1}	3 ab^{-1}
Valid excluded by Higgs couplings	0.023	0.077
Excluded only by Higgs couplings	0.015	0.024
Accepted excluded by Higgs couplings	0.012	0.047
Excluded only by Higgs couplings	0.006	0.019

pMSSM points that can be tested and excluded, assuming that the measured Higgs couplings coincide exactly with those predicted by the SM.

The fraction of points within the range of the scans performed here (see Table II) excluded by the SUSY direct searches (see Table IV) are summarized in Table V. Considering the valid and accepted pMSSM points and following the fractions of those that can be excluded by the Higgs measurements at the LHC, we observe that these fractions range from 1% to 2% and 5% to 8% for the run 2 and HL-LHC datasets, respectively. If we restrict ourselves to considering the points that can be excluded only by the Higgs coupling measurements and are not excluded by the direct SUSY searches (heavy Higgs bosons and scalar quarks, leptons, and gauginos) conducted on the same data sets, these fractions become approximately 1% and 2% (see Table VIII. Despite the increasing accuracy of the Higgs measurements, the fraction of pMSSM points that can be excluded by the Higgs coupling measurements during the LHC program remains small. However, their increase indicates that the improvement of the sensitivity obtained by the Higgs measurements with higher accuracy beats the estimated increase in sensitivity of the direct searches moving from run 2 to the HL-LHC.

The fractions of points excluded by the Higgs couplings at the LHC and at future e^+e^- colliders are presented in Table IX, in relation to the current sensitivity of the direct searches at LHC run 2. The reduction of sensitivity of the Higgs coupling measurements observed for the accepted points, fulfilling the flavor physics constraints, and for the points not excluded by the direct searches comes almost entirely from the exclusion of the low to moderate M_A scenarios in both cases. The exclusion of the pMSSM at moderate values of M_A pushes the h boson into the decoupling regime. The deviations of the Higgs couplings due to the Δ_b effect vanishing in the decoupling regime, the constraints from missing E_T searches on the mass of scalar quarks and gauginos have only a minor effect. By improving the accuracy of these Higgs coupling measurements to the percent, or subpercent, level, as expected at future e^+e^- Higgs factories, the ILC and the FCC-ee, can test up to about 10%–12% of the pMSSM points not excluded by the current LHC direct SUSY searches and flavor physics data (see Table IX), provided they can operate at a large enough energy to perform a full study of the Higgs profile.

B. Extracting MSSM parameters from the Higgs profile

By studying the Higgs couplings as a function of the MSSM parameters for the accepted pMSSM points, we observe four main groups of parameters to which the Higgs couplings are sensitive. In general, these are: M_A, $M_{\tilde{g},\tilde{b},\tilde{t},\tilde{\tau}}$, $\mu \tan\beta$, and $M_{\tilde{\chi}_1^0}$, but this sensitivity is strongly reduced when only the pMSSM points compatible with the LHC run 2 searches are considered.

The small fractions of pMSSM points viable after the run 2 searches that can be excluded by future precision measurements of the Higgs couplings, discussed in the previous section, highlight the decoupling properties of the lightest MSSM Higgs boson, once the value of M_A is constrained to sufficiently large values. In this regime, the

TABLE IX. Fraction of pMSSM points excluded at 90% CL by the Higgs coupling measurements assuming SM central values and the accuracies estimated for the HL-LHC and the e^+e^- ILC and FCC-ee Higgs factory proposals. The fractions excluded by the current LHC run-2 Higgs coupling results are also given in the first column. The first lines of each block gives the fractions of all valid (neutralino LSP + $122 < M_h < 128$ GeV) and accepted (valid + flavor + $\Omega_\chi h^2$) pMSSM points, respectively, followed by the fractions for the points not excluded by the direct searches for H/A heavy Higgs bosons and also by those in the jets and/or leptons + MET channels with the run 2 sensitivity.

| pMSSM	LHC	HL-LHC	ILC	ILC	ILC	FCC-ee	FCC-ee
Selection	140 fb^{-1}	3 ab^{-1}	250 GeV	500 GeV	1 TeV	240 GeV	365 GeV
Valid	0.023	0.077	0.083	0.166	0.191	0.102	0.156
H/A (LHC run-2)	0.017	0.061	0.068	0.115	0.133	0.078	0.108
H/A and j/ℓ + MET (LHC run-2)	0.016	0.059	0.066	0.114	0.130	0.076	0.106
Accepted	0.012	0.048	0.054	0.137	0.161	0.072	0.125
H/A (LHC run-2)	0.012	0.047	0.053	0.107	0.125	0.067	0.098
H/A & j/ℓ + MET (LHC run-2)	0.011	0.046	0.051	0.106	0.123	0.065	0.097
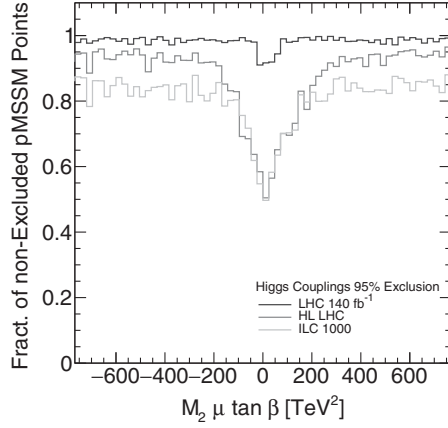
FIG. 10. Fraction of accepted pMSSM points not excluded at the 95% of CL by the Higgs couplings as a function of $M_2\mu\tan\beta$ for the present run 2 ATLAS results (dark grey) and the expected HL-LHC (medium grey) and ILC-1000 (light grey) accuracies, assuming SM central values.

modifications of the Higgs coupling to $b\bar{b}$ as a function of $M_{\tilde{g},\tilde{b},\tilde{t},\tilde{\tau}}$ and $\mu\tan\beta$ through the Δ_b term are suppressed. Among the pMSSM parameters inducing effects on the Higgs couplings, discussed in Secs. II and III, only $M_{\tilde{\chi}_1^0}$, through invisible decays if $M_\chi < 0.5M_h$, and M_A remain viable.

1. $M_{\tilde{\chi}_1^0}$

If $M_\chi < 0.5M_h$ the h can decay to neutralino pairs, as discussed in Sec. II D. The fraction of accepted pMSSM points compatible with the Higgs couplings is shown as a function of $M_2\mu\tan\beta$, relevant to the determination of the Higgs invisible decay rate, in Fig. 10.

Limits on the invisible decay rate can be used to constrain the value of the neutralino LSP mass. As we have already pointed out, the $h\chi\chi$ coupling also controls the χp scattering cross section thus introducing a correlation between the rate of $h \to \chi\chi$, the scattering cross section and the neutralino relic density, $\Omega_{\tilde{\chi}_1^0}$. A large rate for invisible Higgs decays implies a large χp scattering cross section, because they are both due to an enhanced $h\chi\chi$ coupling. This is shown in Fig. 11 visualizing the predicted spin-independent χN scattering cross section on nucleons in the portion of our pMSSM points with low $M_{\tilde{\chi}_1^0}$ values highlighting the points with sizeable $h \to \chi\chi$ branching fractions. Bounds on the χ scattering cross section place nontrivial constraints on the Higgs invisible rate as shown in the upper panel in Fig. 11. These bounds are relaxed but not invalidated even when the predicted scattering cross section is rescaled by the ratio $\Omega_\chi/\Omega_{\rm CDM}$ for points having neutralino relic density significantly lower that the current PLANCK result for $\Omega_{\rm CDM}$ (see the lower panel in Fig. 11). In particular, the XENON-1T upper limit on the scattering cross section on nucleons for neutralino masses below
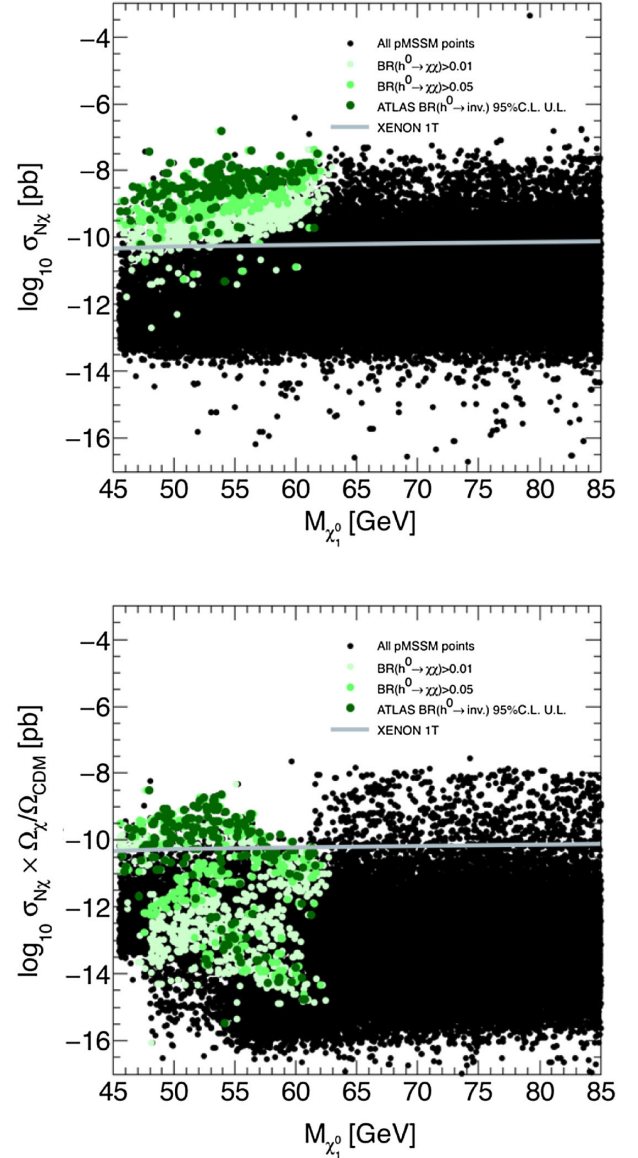

FIG. 11. Predicted spin-independent χN scattering cross section on nucleons, as a function of $M_{\tilde{\chi}_1^0}$ values with highlighted pMSSM points with sizeable $h \to \chi\chi$ branching fractions. Points with sizeable $h \to \chi\chi$ branching fractions are shown in color, the darker shade indicating those with branching fractions exceeding the ATLAS upper bounds on invisible Higgs boson decays [31]. The line represents the upper bound from the XENON 1T data. The lower panel has the χN scattering cross section values rescaled by $\Omega_\chi/\Omega_{\rm CDM}$.

$M_h/2$ from the 1.0 ton-yr exposure [101] removes almost all of the MSSM solutions having BR$(h \to \chi\chi)$ above 0.01 and provides a competitive constraint compared to the direct current upper bound on Higgs invisible decays at 0.11 [28–31] within the MSSM with the lightest neutralino as the only source of dark matter.

This reduces the invisible Higgs rate likely below the sensitivity at the LHC, determined either directly through
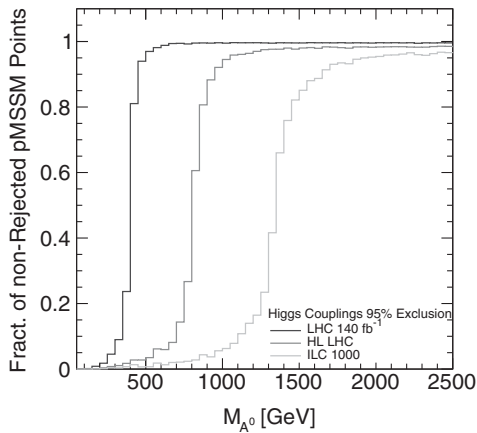
FIG. 12. Fraction of accepted pMSSM points not excluded at the 95% of CL by the Higgs couplings as a function of the M_A mass for the present run 2 ATLAS results (dark grey) and the expected HL-LHC (medium grey) and ILC-1000 (light grey) accuracies, assuming SM central values.

ZH and VBF production or indirectly through the sum of the Higgs rates, and makes it unique to the e^+e^- collider program. In our pMSSM scenario with $M_\chi = 58.3$ GeV, the fit to the Higgs branching fractions makes it possible to indirectly reconstruct the neutralino mass with better than 10% relative statistical accuracy.

2. M_A

The sensitivity to the pseudoscalar Higgs boson mass, M_A, is the main MSSM benchmark for the light Higgs coupling measurements. The scaling of the coupling deviations with M_Z^2/M_A^2 (see Sec. II F) offers us with an opportunity to discriminate a MSSM h from the SM H boson and to infer the mass of the pseudoscalar state from the precision measurements of the properties of the lighter state. The fraction of accepted pMSSM points excluded by the h coupling determination for different accuracies is shown as a function of M_A in Fig. 12. We have verified that our scans contain points corresponding to the so-called "alignment scenario", where small M_A values correspond

to SM-like Higgs couplings [126]. However these points in our scans are removed by flavor data and direct searches at the LHC.

The M_A values at which more than 90% (95%) of the accepted pMSSM points are excluded by the Higgs couplings at 95% CL are 300 (275) GeV for the present run 2 ATLAS data, 675 (525) GeV, and 1075 (925) GeV for the expected HL-LHC and ILC-1000 accuracies assuming SM central values. This picture changes when only the pMSSM points not excluded by the jet/ℓ + MET searches on the LHC run 2 data are considered. These searches remove a significant fraction of points with relatively light pseudoscalars, as discussed in Sec. IV B. These points see different contributions to the Higgs couplings, from M_A as well as from the lighter SUSY particles, resulting in a spread of the values of the couplings. Once these points are largely removed, the dependence of the Higgs couplings on M_A becomes dominant, and the bounds on M_A are improved. The M_A values at which more than 90% (95%) of the pMSSM points not excluded by the SUSY searches as listed in Table IV are excluded by the Higgs couplings at 95% CL are 350 (325) GeV for the present run 2 ATLAS data, 750 (725) GeV and 1225 (1165) GeV for the expected HL-LHC and ILC-1000 accuracies assuming again SM central values. By the end of the LHC program, if no deviation from the SM prediction is observed, the Higgs couplings will probe M_A up to 750 GeV. Owing to its improved accuracy, an e^+e^- Higgs factory is expected to extend this indirect sensitivity up to heavy Higgs boson masses of $\simeq 1200$ GeV (see Fig. 13). This reach is comparable to that of the direct H/A searches at the HL-LHC, discussed in Sec. IV B (see Fig. 6). As expected, the errors on the reconstructed mass increase with the M_A value.

Further, the accurate determination of the h couplings can be used to estimate M_A, in the case the measured values significantly deviate from the SM predictions. We evaluate the accuracy of this estimate as a function of the value of M_A by considering a set of benchmark scenarios, not excluded by run 2 data, summarized in Table X. The h couplings and branching fractions are computed for these benchmarks and compared to the value for our accepted
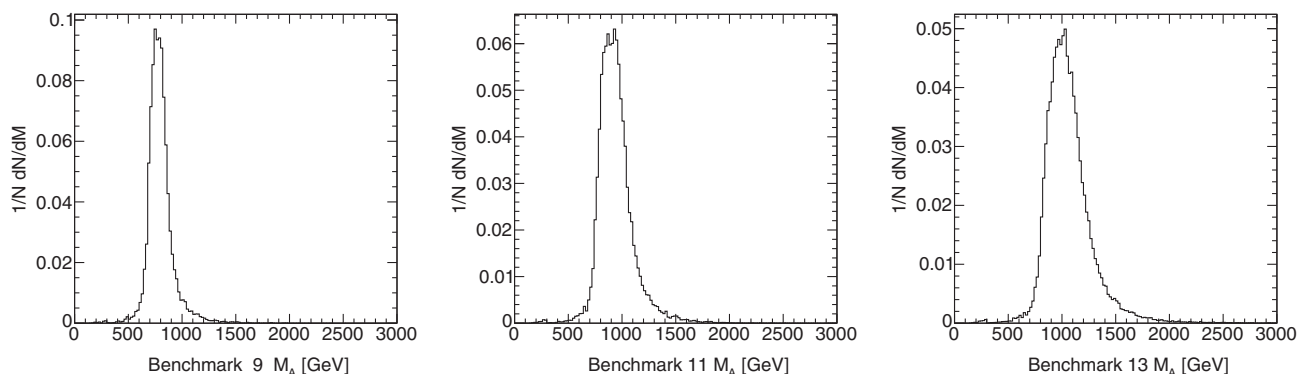

FIG. 13. Probability density function for M_A corresponding to the ILC 1000 accuracy obtained for the benchmark points 9, 11, and 13.

TABLE X.   pMSSM scenarios adopted in the study of the extraction of M_A.

Scenario	M_A (GeV)	$\tan\beta$	μ (GeV)	$M_{\tilde{t}_1}$ (GeV)	$M_{\tilde{\tau}_1}$ (GeV)	$M_{\tilde{\chi}_1^0}$ (GeV)	$M_{\tilde{\chi}_1^\pm}$ (GeV)	$M_{\tilde{g}}$ (GeV)
1	285	6.4	−12.2	4023	1546	3.3	14.9	5204
2	434	5.6	−549	1493	744	562	564	5059
3	472	6.6	1994	1652	1407	315	1459	390
4	510	5.5	−181	3749	1999	185	186	4585
5	554	6.5	2351	4613	2294	737	2012	4379
6	606	6.3	369	3688	1510	380	381	3571
7	649	5.7	−1411	1886	1178	444	445	2961
8	704	5.2	480	4924	865	170	493	3436
9	747	4.5	−3596	3483	3080	1072	1073	2324
10	798	5.8	−3302	2712	2258	1329	3284	2085
11	844	9.1	−1679	1902	2045	1695	1696	4502
12	893	7.1	−368	5038	2095	379	381	2889
13	947	7.7	−4268	2941	2276	364	3677	441
14	1002	5.4	716	3037	827	732	733	3234
15	1095	12.0	1330	3068	4060	1351	1352	5722

pMSSM points in the scan. Each point is assigned a weight defined as the χ^2 probability of the point with the scenario tested, where the χ^2 is computed using the Higgs coupling modifiers with the accuracies for the LHC and the e^+e^- Higgs factories given in Table VII. The values of M_A of these weighted points give distributions (some of which are shown in Fig. 13) from which the central value and uncertainty of the M_A parameters are extracted. The central values are computed as the average in an interval integrating 68% of the entries around the most probable value. The uncertainties are obtained by determining the interval of parameter values around the central value, which integrates 68% of the weighted entries allowing for asymmetric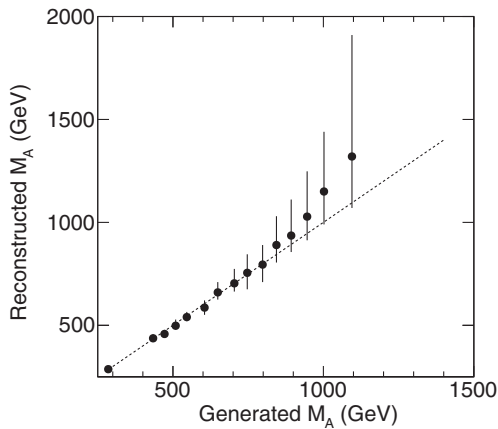 ranges. The relation between the generated and reconstructed values of M_A for the chosen benchmark points is shown in Fig. 14.

VI. CONCLUSIONS

The study of the Higgs boson properties offers compelling perspectives for testing the effects of physics beyond the Standard Model at the LHC and at future colliders. This is particularly the case in the context of supersymmetric theories and its minimal version, the MSSM. The Higgs couplings to SM particles, both at tree level and through loops, are sensitive to new physics effects and can be used to discriminate the MSSM h from the SM H.

In this study, we have reviewed the SUSY corrections to the couplings and decay rates of the SM-like Higgs boson and their dependence on the MSSM parameters. The constraints and predictivity of the Higgs measurements are applied directly on the relevant supersymmetric parameters using scans of the pMSSM parameter space and contrasted with those derived from direct searches for new particles at the LHC. Theoretical and parametric uncertainties in Higgs production and decay also need to be considered alongside the experimental accuracies. These are revisited and discussed in detail.

The sources of these corrections can be classified in three main categories: the pseudoscalar Higgs mass M_A, the invisible decays $h \to \tilde{\chi}^0\tilde{\chi}^0$, $\tilde{\nu}\tilde{\nu}$, and the SUSY–QCD corrections generating the Δ_b, Δ_t, and Δ_τ terms through scalar quarks and gluino or scalar tau and gaugino-Higgsino contributions.

The values of the lightest neutralino mass as well as the Higgsino and gaugino mass parameters, μ and M_1, M_2, that can generate significant rates of invisible decays are already constrained by dark matter direct detection data, even more

FIG. 14.   Reconstructed most probable value vs generated value of M_A for the study points. The deviation of the reconstructed most probable value from the diagonal at large values of M_A is due to the loss of sensitivity on the lower side of the M_A probability density distribution.

severely than by the results of the current LHC invisible Higgs decay searches. For the range of M_A values not yet probed by the ATLAS and CMS data or excluded by flavor data, the Δ_b contribution to the light h boson coupling to $b\bar{b}$ is largely reduced, by compensation of direct and indirect contributions, and the remaining one-loop SUSY corrections are tiny. The effects of the Δ_t and Δ_τ corrections are in general small. This reduces the sensitivity of Higgs couplings and decay rates to MSSM parameters other than M_A as the main MSSM parameter that can be probed in the continuation of the LHC program and at future e^+e^- colliders.

This study has shown that Higgs coupling measurements with the accuracies obtained on the LHC run 2 data and those expected for the HL-LHC and future e^+e^- colliders can exclude ∼2%, 8%, and 20%, respectively, of the accepted pMSSM points in our scans, but only ∼1%, 5%, and 12% of the points that are not yet excluded by flavor data and by the LHC heavy Higgs direct searches, while direct SUSY searches have only a mild impact. The indirect sensitivity to M_A in the pMSSM through the Higgs coupling measurements will evolve from ∼450 GeV for the run 2 data to ∼800 GeV at HL-LHC and ∼1400 GeV at future e^+e^- colliders. Within this range, future e^+e^- colliders of sufficient energy can indirectly determine M_A to a relative accuracy ranging from ≃8% to 40% for M_A values from 700 GeV to 1.1 TeV, from the deviations of the measured lightest h couplings with respect to their SM expectations.

Thus, large parts of the MSSM parameters are still to be probed and the statement that the properties of the observed Higgs boson are SM-like, often used when discussing the present LHC results, could also be rephrased by saying that they are also MSSM-like.

ACKNOWLEDGMENTS

[1] The ATLAS Collaboration, Phys. Lett. B **716**, 1 (2012); The CMS Collaboration, Phys. Lett. B **716**, 30 (2012).

[2] P. W. Higgs, Phys. Lett. **12**, 132 (1964); Phys. Rev. Lett. **13**, 508 (1964); Phys. Rev. **145**, 1156 (1966); F. Englert and R. Brout, Phys. Rev. Lett. **13**, 321 (1964); G. S. Guralnik, C. R. Hagen, and T. W. Kibble, Phys. Rev. Lett. **13**, 585 (1964); T. W. B. Kibble, Phys. Rev. **155**, 1554 (1967).

[3] The ATLAS and CMS Collaborations, J. High Energy Phys. 08 (2016) 045; The ATLAS Collaboration, Report No. ATLAS-CONF-2019-005; The CMS Collaboration, J. High Energy Phys. 01 (2021) 148.

[4] Y. A. Golfand and E. P. Likhtman, Pis'ma Zh. Eksp. Teor. Fiz. **13**, 452 (1971) [JETP Lett. **13**, 323 (1971)]; D. V. Volkov and V. P. Akulov, Phys. Lett. **46B**, 109 (1973); J. Wess and B. Zumino, Nucl. Phys. **B70**, 39 (1974).

[5] For reviews on supersymmetric theories, see P. Fayet and S. Ferrara, Phys. Rep. **32**, 249 (1977); H. P. Nilles, Phys. Rep. **110**, 1 (1984); R. Barbieri, Riv. Nuovo Cimento **11N4**, 1 (1988); M. Drees, R. Godbole, and P. Roy, *Theory and Phenomenology of Sparticles* (World Scientific, Singapore, 2005); H. Baer and X. Tata, *Weak Scale Supersymmetry: From Superfields to Scattering Events* (Cambridge University Press, Cambridge, England, 2006); S. Martin, Adv. Ser. Dir. High Energy Phys. **18**, 1 (1998); P. Binétruy, *Supersymmetry: Theory, Experiment, and Cosmology* (Oxford University Press, New York, 2006).

[6] H. E. Haber and G. L. Kane, Phys. Rep. **117**, 75 (1985).

[7] M. Kakizaki, S. Kanemura, M. Kikuchi, T. Matsui, and H. Yokoya, Int. J. Mod. Phys. A **30**, 1550192 (2015); J. Baglio, A. Djouadi, and J. Quevillon, Rep. Prog. Phys. **79**, 116201 (2016); P. Athron *et al.* (GAMBIT Collaboration), Eur. Phys. J. C **77**, 824 (2017); **77**, 879 (2017); E. Bagnaschi *et al.*, Eur. Phys. J. C **78**, 256 (2018); E. Bagnaschi, H. Bahl, J. Ellis, J. Evans, T. Hahn, S. Heinemeyer, W. Hollik, K. A. Olive, S. Paßehr, H. Rzehak *et al.*, Eur. Phys. J. C **79**, 149 (2019).

[8] A. Djouadi *et al.*, arXiv:hep-ph/9901246.

[9] Y. Okada, M. Yamaguchi, and T. Yanagida, Prog. Theor. Phys. **85**, 1 (1991); J. Ellis, G. Ridolfi, and F. Zwirner, Phys. Lett. B **257**, 83 (1991); H. Haber and R. Hempfling, Phys. Rev. Lett. **66**, 1815 (1991).

[10] M. Carena, J. Espinosa, M. Quiros, and C. E. M. Wagner, Phys. Lett. B **355**, 209 (1995); M. Carena, M. Quiros, and C. E. M. Wagner, Nucl. Phys. **B461**, 407 (1996).

[11] H. Haber, R. Hempfling, and A. Hoang, Z. Phys. C **75**, 539 (1997).

[12] S. Heinemeyer, W. Hollik, and G. Weiglein, Phys. Rev. D **58**, 091701 (1998); Eur. Phys. J. C **9**, 343 (1999); G. Degrassi, P. Slavich, and F. Zwirner, Nucl. Phys. **B611**, 403 (2001); A. Brignole, G. Degrassi, P. Slavich, and F. Zwirner, Nucl. Phys. **B631**, 195 (2002); **B643**, 79 (2002); B. Allanach, A. Djouadi, J. L. Kneur, W. Porod, and P. Slavich, J. High Energy Phys. 09 (2004) 044; S. Martin, Phys. Rev. D **75**, 055005 (2007); P. Kant, R. Harlander, L. Mihaila, and M. Steinhauser, J. High Energy Phys. 08 (2010) 104.

[13] S. P. Martin, Phys. Rev. D **75**, 055005 (2007); R. V. Harlander, P. Kant, L. Mihaila, and M. Steinhauser, Phys. Rev. Lett. **100**, 191602 (2008); **101**, 039901(E) (2008);

N. Bernal, A. Djouadi, and P. Slavich, J. High Energy Phys. 07 (2007) 016; P. Draper, G. Lee, and C. E. M. Wagner, Phys. Rev. D **89**, 055023 (2014); E. Bagnaschi, G. F. Giudice, P. Slavich, and A. Strumia, J. High Energy Phys. 09 (2014) 092; K. Cheung, R. Huo, J. S. Lee, and Y. L. Sming Tsai, J. High Energy Phys. 04 (2015) 151; J. Pardo Vega and G. Villadoro, J. High Energy Phys. 07 (2015) 159; H. Bahl and W. Hollik, Eur. Phys. J. C **76**, 499 (2016); P. Slavich, S. Heinemeyer, E. Bagnaschi, H. Bahl, M. Goodsell, H. E. Haber, T. Hahn, R. Harlander, W. Hollik, G. Lee *et al.*, Eur. Phys. J. C **81**, 450 (2021).

[14] M. Carena and H. Haber, Prog. Part. Nucl. Phys. **50**, 63 (2003); S. Heinemeyer, W. Hollik, and G. Weiglein, Phys. Rep. **425**, 265 (2006); S. Heinemeyer, Int. J. Mod. Phys. A **21**, 2659 (2006).

[15] G. Lee and C. E. M. Wagner, Phys. Rev. D **92**, 075032 (2015).

[16] M. Carena, S. Heinemeyer, O. Stål, C. E. M. Wagner, and G. Weiglein, Eur. Phys. J. C **73**, 2552 (2013).

[17] A. Djouadi, L. Maiani, G. Moreau, A. Polosa, J. Quevillon, and V. Riquer, Eur. Phys. J. C **73**, 2650 (2013).

[18] L. Maiani, A. D. Polosa, and V. Riquier, New J. Phys. **14**, 073029 (2012); Phys. Lett. B **718**, 465 (2012); **724**, 274 (2013); A. Djouadi and J. Quevillon, J. High Energy Phys. 10 (2013) 028.

[19] A. Djouadi, L. Maiani, A. Polosa, J. Quevillon, and V. Riquer, J. High Energy Phys. 06 (2015) 168.

[20] A. Brignole, Phys. Lett. B **277**, 313 (1992); M. Frank, L. Galeta, T. Hahn, S. Heinemeyer, W. Hollik, H. Rzehak, and G. Weiglein, Phys. Rev. D **88**, 055013 (2013).

[21] The ATLAS Collaboration, Phys. Lett. B **812**, 135980 (2021).

[22] The CMS Collaboration, Report No. CMS-PAS-HIG-19-006.

[23] A. Djouadi, J. Kalinowski, and M. Spira, Comput. Phys. Commun. **108**, 56 (1998); A. Djouadi, M. M. Mühlleitner, and M. Spira, Acta Phys. Pol. B **38**, 635 (2007); A. Djouadi, J. Kalinowski, M. Mühlleitner, and M. Spira, Comput. Phys. Commun. **238**, 214 (2019).

[24] H. Baer, A. Belyaev, T. Krupovnickas, and A. Mustafayev, J. High Energy Phys. 06 (2004) 044; A. Djouadi, M. Drees, and J. L. Kneur, Phys. Lett. B **624**, 60 (2005); For a recent discussion, see G. Arcadi, A. Djouadi, and M. Raidal, Phys. Rep. **842**, 1 (2020).

[25] A. Arbey, M. Battaglia, A. Djouadi, F. Mahmoudi, and J. Quevillon, Phys. Lett. B **708**, 162 (2012); **720**, 153 (2013); J. High Energy Phys. 09 (2012) 107.

[26] P. A. Zyla *et al.* (Particle Data Group), Prog. Theor. Exp. Phys. **2020**, 083C01 (2020).

[27] A. Djouadi and M. Drees, Phys. Lett. B **407**, 243 (1997).

[28] The CMS Collaboration, Phys. Lett. B **793**, 520 (2019).

[29] The ATLAS Collaboration, Phys. Rev. Lett. **122**, 231801 (2019).

[30] The ATLAS Collaboration, Report No. ATLAS-CONF-2020-008.

[31] The ATLAS Collaboration, Report No. ATLAS-CONF-2020-052.

[32] J. Fleischer and F. Jegerlehner, Phys. Rev. D **23**, 2001 (1981); D. Y. Bardin, B. M. Vilensky, and P. K. Khristova, Yad. Fiz. **53**, 240 (1991) [Sov. J. Nucl. Phys. **53**, 152 (1991)]; A. Dabelstein and W. Hollik, Z. Phys. C **53**, 507 (1992); B. A. Kniehl, Nucl. Phys. **B376**, 3 (1992).

[33] A. Dabelstein, Nucl. Phys. **B456**, 25 (1995).

[34] E. Braaten and J. P. Leveille, Phys. Rev. D **22**, 715 (1980); N. Sakai, Phys. Rev. D **22**, 2220 (1980); T. Inami and T. Kubota, Nucl. Phys. **B179**, 171 (1981); M. Drees and K.-I. Hikasa, Phys. Rev. D **41**, 1547 (1990); Phys. Lett. B **240**, 455 (1990); **262**, 497(E) (1991); S. G. Gorishnii, A. L. Kataev, S. A. Larin, and L. R. Surguladze, Mod. Phys. Lett. A **05**, 2703 (1990); S. G. Gorishnii, A. L. Kataev, S. A. Larin, and L. R. Surguladze, Phys. Rev. D **43**, 1633 (1991); A. L. Kataev and V. T. Kim, Mod. Phys. Lett. A **09**, 1309 (1994); S. G. Gorishnii, A. L. Kataev, and S. A. Larin, Yad. Fiz. **40**, 517 (1984) [Sov. J. Nucl. Phys. **40**, 329 (1984)]; L. R. Surguladze, Phys. Lett. B **341**, 60 (1994); S. A. Larin, T. van Ritbergen, and J. A. M. Vermaseren, Phys. Lett. B **362**, 134 (1995); K. G. Chetyrkin and A. Kwiatkowski, Nucl. Phys. **B461**, 3 (1996); K. G. Chetyrkin, Phys. Lett. B **390**, 309 (1997); P. A. Baikov, K. G. Chetyrkin, and J. H. Kühn, Phys. Rev. Lett. **96**, 012003 (2006).

[35] J. A. Coarasa, R. A. Jimenez, and J. Solà, Phys. Lett. B **389**, 312 (1996); H. Eberl, K. Hidaka, S. Kraml, W. Majerotto, and Y. Yamada, Phys. Rev. D **62**, 055006 (2000).

[36] L. J. Hall, R. Rattazzi, and U. Sarid, Phys. Rev. D **50**, 7048 (1994); R. Hempfling, Phys. Rev. D **49**, 6168 (1994); M. Carena, M. Olechowski, S. Pokorski, and C. E. M. Wagner, Nucl. Phys. **B426**, 269 (1994); D. M. Pierce, J. A. Bagger, K. T. Matchev, and R.-J. Zhang, Nucl. Phys. **B491**, 3 (1997); J. Guasch, W. Hollik, and S. Penaranda, Phys. Lett. B **515**, 367 (2001); G. D'Ambrosio, G. F. Giudice, G. Isidori, and A. Strumia, Nucl. Phys. **B645**, 155 (2002); A. J. Buras, P. H. Chankowski, J. Rosiek, and L. Slawianowska, Nucl. Phys. **B659**, 3 (2003); V. Barger, H. E. Logan, and G. Shaughnessy, Phys. Rev. D **79**, 115018 (2009); N. D. Christensen, T. Han, and S. Su, Phys. Rev. D **85**, 115018 (2012).

[37] M. S. Carena, D. Garcia, U. Nierste, and C. E. M. Wagner, Nucl. Phys. **B577**, 88 (2000).

[38] J. Guasch, P. Häfliger, and M. Spira, Phys. Rev. D **68**, 115001 (2003).

[39] D. Noth and M. Spira, Phys. Rev. Lett. **101**, 181801 (2008); J. High Energy Phys. 06 (2011) 084; L. Mihaila and C. Reisser, J. High Energy Phys. 08 (2010) 021; A. Crivellin and C. Greub, Phys. Rev. D **87**, 015013 (2013); **87**, 079901(E) (2013); L. Mihaila and N. Zerf, J. High Energy Phys. 05 (2017) 019; M. Ghezzi, S. Glaus, D. Müller, T. Schmidt, and M. Spira, Eur. Phys. J. C **81**, 259 (2021).

[40] H. Q. Zheng and D. D. Wu, Phys. Rev. D **42**, 3760 (1990); A. Djouadi, M. Spira, J. J. van der Bij, and P. M. Zerwas, Phys. Lett. B **257**, 187 (1991); S. Dawson and R. P. Kauffman, Phys. Rev. D **47**, 1264 (1993); A. Djouadi, M. Spira, and P. M. Zerwas, Phys. Lett. B **311**, 255 (1993); K. Melnikov and O. I. Yakovlev, Phys. Lett. B **312**, 179 (1993); M. Inoue, R. Najima, T. Oka, and J. Saito, Mod. Phys. Lett. A **09**, 1189 (1994); M. Steinhauser, arXiv:hep-ph/9612395; J. Fleischer, O. V. Tarasov, and V. O. Tarasov, Phys. Lett. B **584**, 294 (2004); M. Mühlleitner and M. Spira, Nucl. Phys. **B790**, 1 (2008); P. Maierhöfer and

P. Marquard, Phys. Lett. B **721**, 131 (2013); C. Sturm, Eur. Phys. J. C **74**, 2978 (2014).

[41] G. Degrassi and F. Maltoni, Nucl. Phys. **B724**, 183 (2005); G. Passarino, C. Sturm, and S. Uccirati, Phys. Lett. B **655**, 298 (2007); S. Actis, G. Passarino, C. Sturm, and S. Uccirati, Phys. Lett. B **669**, 62 (2008); Nucl. Phys. **B811**, 182 (2009).

[42] M. Spira, A. Djouadi, and P. M. Zerwas, Phys. Lett. B **276**, 350 (1992); T. Gehrmann, S. Guns, and D. Kara, J. High Energy Phys. 09 (2015) 038; R. Bonciani, V. Del Duca, H. Frellesvig, J. M. Henn, F. Moriello, and V. A. Smirnov, J. High Energy Phys. 08 (2015) 10.

[43] U. Aglietti, R. Bonciani, G. Degrassi, and A. Vicini, Phys. Lett. B **595**, 432 (2004); arXiv:hep-ph/0610033; G. Degrassi and F. Maltoni, Phys. Lett. B **600**, 255 (2004); S. Actis, G. Passarino, C. Sturm, and S. Uccirati, Phys. Lett. B **670**, 12 (2008); Nucl. Phys. **B811**, 182 (2009).

[44] T. Inami, T. Kubota, and Y. Okada, Z. Phys. C **18**, 69 (1983); A. Djouadi, M. Spira, and P. M. Zerwas, Phys. Lett. B **264**, 440 (1991); M. Spira, A. Djouadi, D. Graudenz, and P. M. Zerwas, Nucl. Phys. **B453**, 17 (1995); K. G. Chetyrkin, B. A. Kniehl, and M. Steinhauser, Phys. Rev. Lett. **79**, 353 (1997); P. A. Baikov and K. G. Chetyrkin, Phys. Rev. Lett. **97**, 061803 (2006); F. Herzog, B. Ruijl, T. Ueda, J. A. M. Vermaseren, and A. Vogt, J. High Energy Phys. 08 (2017) 113.

[45] See e.g., M. Spira, Fortschr. Phys. **46**, 203 (1998); Prog. Part. Nucl. Phys. **95**, 98 (2017); A. Djouadi, Phys. Rep. **459**, 1 (2008).

[46] A. Brignole and F. Zwirner, Phys. Lett. B **299**, 72 (1993); K. Williams and G. Weiglein, Phys. Lett. B **660**, 217 (2008); G. Chalons, A. Djouadi, and J. Quevillon, Phys. Lett. B **780**, 74 (2018); S. Liebler, M. Mühlleitner, M. Spira, and M. Stadelmaier, Eur. Phys. J. C **79**, 65 (2019).

[47] A. Djouadi, P. Janot, J. Kalinowski, and P. M. Zerwas, Phys. Lett. B **376**, 220 (1996); A. Djouadi, J. Kalinowski, P. Ohmann, and P. M. Zerwas, Z. Phys. C **74**, 93 (1997).

[48] See e.g., G. Degrassi, S. Heinemeyer, W. Hollik, P. Slavich, and G. Weiglein, Eur. Phys. J. C **28**, 133 (2003); S. Martin, Phys. Rev. D **75**, 055005 (2007); P. Kant, R. Harlander, L. Mihaila, and M. Steinhauser, J. High Energy Phys. 08 (2010) 104; R. V. Harlander, J. Klappert, and A. Voigt, Eur. Phys. J. C **77**, 814 (2017).

[49] S. Heinemeyer *et al.* (LHC Higgs Cross Section Working Group), arXiv:1307.1347.

[50] E. Bagnaschi *et al.*, Report No. LHCHXSWG-2015-002.

[51] A. Djouadi, Eur. Phys. J. C **73**, 2498 (2013); A. Djouadi, J. Quevillon, and R. Vega-Morales, Phys. Lett. B **757**, 412 (2016).

[52] A. Bredenstein, A. Denner, S. Dittmaier, and M. M. Weber, Phys. Rev. D **74**, 013004 (2006); J. High Energy Phys. 02 (2007) 080.

[53] W. Hollik and J. H. Zhang, Phys. Rev. D **84**, 055022 (2011).

[54] K. G. Chetyrkin, J. H. Kühn, A. Maier, P. Maierhofer, P. Marquard, M. Steinhauser, and C. Sturm, Phys. Rev. D **80**, 074010 (2009).

[55] A. Djouadi, M. Spira, and P. M. Zerwas, Z. Phys. C **70**, 427 (1996); E. Gross, G. Wolf, and B. A. Kniehl, Z. Phys. C **63**, 417 (1994); **66**, 321(E) (1995); A. Denner, S. Heinemeyer, I. Puljak, D. Rebuzzi, and M. Spira, Eur. Phys. J. C **71**, 1753 (2011).

[56] D. de Florian *et al.* (LHC Higgs Cross Section Working Group), arXiv:1610.07922.

[57] A. Djouadi, M. Spira, and P. M. Zerwas, Phys. Lett. B **264**, 440 (1991); S. Dawson, Nucl. Phys. **B359**, 283 (1991); D. Graudenz, M. Spira, and P. M. Zerwas, Phys. Rev. Lett. **70**, 1372 (1993); M. Spira, A. Djouadi, D. Graudenz, and P. M. Zerwas, Phys. Lett. B **318**, 347 (1993); M. Spira, A. Djouadi, D. Graudenz, and P. M. Zerwas, Nucl. Phys. **B453**, 17 (1995); R. Harlander and P. Kant, J. High Energy Phys. 12 (2005) 015; C. Anastasiou, S. Bucherer, and Z. Kunszt, J. High Energy Phys. 10 (2009) 068.

[58] S. Catani, D. de Florian, and M. Grazzini, J. High Energy Phys. 05 (2001) 025; R. V. Harlander and W. B. Kilgore, Phys. Rev. D **64**, 013015 (2001); Phys. Rev. Lett. **88**, 201801 (2002); C. Anastasiou and K. Melnikov, Nucl. Phys. **B646**, 220 (2002); V. Ravindran, J. Smith, and W. L. van Neerven, Nucl. Phys. **B665**, 325 (2003); S. Marzani, R. D. Ball, V. Del Duca, S. Forte, and A. Vicini, Nucl. Phys. **B800**, 127 (2008); R. V. Harlander and K. J. Ozeren, Phys. Lett. B **679**, 467 (2009); J. High Energy Phys. 11 (2009) 088; A. Pak, M. Rogal, and M. Steinhauser, Phys. Lett. B **679**, 473 (2009); A. Pak, M. Rogal, and M. Steinhauser, J. High Energy Phys. 02 (2010) 025.

[59] T. Gehrmann, M. Jaquier, E. W. N. Glover, and A. Koukoutsakis, J. High Energy Phys. 02 (2012) 056; C. Anastasiou, C. Duhr, F. Dulat, and B. Mistlberger, J. High Energy Phys. 07 (2013) 003; C. Anastasiou, C. Duhr, F. Dulat, F. Herzog, and B. Mistlberger, J. High Energy Phys. 12 (2013) 088; W. B. Kilgore, Phys. Rev. D **89**, 073008 (2014); Y. Li, A. von Manteuffel, R. M. Schabinger, and H. X. Zhu, Phys. Rev. D **90**, 053006 (2014); C. Anastasiou, C. Duhr, F. Dulat, E. Furlan, T. Gehrmann, F. Herzog, and B. Mistlberger, J. High Energy Phys. 03 (2015) 091; C. Anastasiou, C. Duhr, F. Dulat, F. Herzog, and B. Mistlberger, Phys. Rev. Lett. **114**, 212001 (2015); C. Anastasiou, C. Duhr, F. Dulat, E. Furlan, T. Gehrmann, F. Herzog, A. Lazopoulos, and B. Mistlberger,ʻ J. High Energy Phys. 05 (2016) 058; B. Mistlberger, J. High Energy Phys. 05 (2018) 028.

[60] M. Krämer, E. Laenen, and M. Spira, Nucl. Phys. **B511**, 523 (1998); S. Catani, D. de Florian, M. Grazzini, and P. Nason, J. High Energy Phys. 07 (2003) 028; S. Moch and A. Vogt, Phys. Lett. B **631**, 48 (2005); V. Ravindran, Nucl. Phys. **B746**, 58 (2006); **B752**, 173 (2006); A. Idilbi, X. d. Ji, J. P. Ma, and F. Yuan, Phys. Rev. D **73**, 077501 (2006); V. Ahrens, T. Becher, M. Neubert, and L. L. Yang, Eur. Phys. J. C **62**, 333 (2009); D. de Florian and M. Grazzini, Phys. Lett. B **674**, 291 (2009); D. de Florian and M. Grazzini, Phys. Lett. B **718**, 117 (2012); D. de Florian, J. Mazzitelli, S. Moch, and A. Vogt, J. High Energy Phys. 10 (2014) 176; M. Bonvini and L. Rottoli, Phys. Rev. D **91**, 051301 (2015); S. Catani, L. Cieri, D. de Florian, G. Ferrera, and M. Grazzini, Nucl. Phys. **B888**, 75 (2014); M. Bonvini and S. Marzani, J. High Energy Phys. 09 (2014) 007; T. Schmidt and M. Spira, Phys. Rev. D **93**, 014022 (2016); M. Bonvini, S. Marzani, C. Muselli, and L. Rottoli, J. High Energy Phys. 08 (2016) 105.

[61] M. Czakon, R. V. Harlander, J. Klappert, and M. Niggetiedt, Phys. Rev. Lett. **127,** 162002 (2021).

[62] C. Anastasiou, R. Boughezal, and F. Petriello, J. High Energy Phys. 04 (2009) 003; M. Bonetti, K. Melnikov, and L. Tancredi, Phys. Rev. D **97,** 034004 (2018); **97,** 056017 (2018); **97,** 099906(e) (2018); C. Anastasiou, V. del Duca, E. Furlan, B. Mistlberger, F. Moriello, A. Schweitzer, and C. Specchia, J. High Energy Phys. 03 (2019) 162.

[63] J. Baglio and A. Djouadi, J. High Energy Phys. 03 (2011) 055; 10 (2010) 064.

[64] S. Dittmaier *et al.,* arXiv:1201.3084.

[65] T. Han, G. Valencia, and S. Willenbrock, Phys. Rev. Lett. **69,** 3274 (1992); T. Figy, C. Oleari, and D. Zeppenfeld, Phys. Rev. D **68,** 073005 (2003); T. Figy and D. Zeppenfeld, Phys. Lett. B **591,** 297 (2004); E. L. Berger and J. M. Campbell, Phys. Rev. D **70,** 073011 (2004).

[66] P. Bolzoni, F. Maltoni, S. O. Moch, and M. Zaro, Phys. Rev. Lett. **105,** 011801 (2010); Phys. Rev. D **85,** 035002 (2012); M. Cacciari, F. A. Dreyer, A. Karlberg, G. P. Salam, and G. Zanderighi, Phys. Rev. Lett. **115,** 082002 (2015); **120,** 139901(E) (2018); R. V. Harlander, J. Vollinga, and M. M. Weber, Phys. Rev. D **77,** 053010 (2008); J. R. Andersen, T. Binoth, G. Heinrich, and J. M. Smillie, J. High Energy Phys. 02 (2008) 057; A. Bredenstein, K. Hagiwara, and B. Jäger, Phys. Rev. D **77,** 073004 (2008); G. Ferrera, M. Grazzini, and F. Tramontano, J. High Energy Phys. 04 (2014) 039; Phys. Lett. B **740,** 51 (2015); F. A. Dreyer and A. Karlberg, Phys. Rev. Lett. **117,** 072001 (2016).

[67] M. Ciccolini, A. Denner, and S. Dittmaier, Phys. Rev. Lett. **99,** 161803 (2007); Phys. Rev. D **77,** 013002 (2008).

[68] J. M. Campbell, R. K. Ellis, and G. Zanderighi, J. High Energy Phys. 10 (2006) 028; J. M. Campbell, R. K. Ellis, and C. Williams, Phys. Rev. D **81,** 074023 (2010).

[69] T. Han and S. Willenbrock, Phys. Lett. B **273,** 167 (1991).

[70] O. Brein, A. Djouadi, and R. Harlander, Phys. Lett. B **579,** 149 (2004).

[71] M. L. Ciccolini, S. Dittmaier, and M. Krämer, Phys. Rev. D **68,** 073003 (2003); A. Denner, S. Dittmaier, S. Kallweit, and A. Mück, J. High Energy Phys. 03 (2012) 075.

[72] L. Altenkamp, S. Dittmaier, R. V. Harlander, H. Rzehak, and T. J. E. Zirke, J. High Energy Phys. 02 (2013) 078; A. Hasselhuhn, T. Luthe, and M. Steinhauser, J. High Energy Phys. 01 (2017) 073; L. Chen, G. Heinrich, S. P. Jones, M. Kerner, J. Klappert, and J. Schlenk, J. High Energy Phys. 03 (2021) 125; J. Davies, G. Mishima, and M. Steinhauser, J. High Energy Phys. 03 (2021) 034; L. Alasfar, G. Degrassi, P. P. Giardino, R. Gröber, and M. Vitti, J. High Energy Phys. 05 (2021) 168; G. Wang, X. Xu, Y. Xu, and L. L. Yang, Phys. Lett. B **829,** 137087 (2022).

[73] W. Beenakker, S. Dittmaier, M. Krämer, B. Plümper, M. Spira, and P. M. Zerwas, Phys. Rev. Lett. **87,** 201805 (2001); Nucl. Phys. **B653,** 151 (2003); L. Reina and S. Dawson, Phys. Rev. Lett. **87,** 201804 (2001); S. Dawson, L. H. Orr, L. Reina, and D. Wackeroth, Phys. Rev. D **67,** 071503 (2003); R. Frederix, S. Frixione, V. Hirschi, F. Maltoni, R. Pittau, and P. Torrielli, Phys. Lett. B **701,** 427 (2011); M. V. Garzelli, A. Kardos, C. G. Papadopoulos, and Z. Trocsanyi, Europhys. Lett. **96,** 11001 (2011); H. B. Hartanto, B. Jäger, L. Reina, and D. Wackeroth, Phys. Rev.

D **91,** 094003 (2015); F. Cascioli, S. Höche, F. Krauss, P. Maierhöfer, S. Pozzorini, and F. Siegert, J. High Energy Phys. 01 (2014) 046; A. Denner and R. Feger, J. High Energy Phys. 11 (2015) 209.

[74] Y. Zhang, W. G. Ma, R. Y. Zhang, C. Chen, and L. Guo, Phys. Lett. B **738,** 1 (2014); S. Frixione, V. Hirschi, D. Pagani, H. S. Shao, and M. Zaro, J. High Energy Phys. 09 (2014) 065; 06 (2015) 184.

[75] A. Kulesza, L. Motyka, T. Stebel, and V. Theeuwes, J. High Energy Phys. 03 (2016) 065; A. Broggio, A. Ferroglia, B. D. Pecjak, A. Signer, and L. L. Yang, J. High Energy Phys. 03 (2016) 124; A. Broggio, A. Ferroglia, B. D. Pecjak, and L. L. Yang, J. High Energy Phys. 02 (2017) 126.

[76] S. Dittmaier, M. Krämer, and M. Spira, Phys. Rev. D **70,** 074010 (2004); S. Dawson, C. B. Jackson, L. Reina, and D. Wackeroth, Phys. Rev. D **69,** 074027 (2004); M. Wiesemann, R. Frederix, S. Frixione, V. Hirschi, F. Maltoni, and P. Torrielli, J. High Energy Phys. 02 (2015) 132.

[77] D. Dicus, T. Stelzer, Z. Sullivan, and S. Willenbrock, Phys. Rev. D **59,** 094016 (1999); C. Balazs, H. J. He, and C. P. Yuan, Phys. Rev. D **60,** 114001 (1999); R. V. Harlander and W. B. Kilgore, Phys. Rev. D **68,** 013001 (2003); C. Duhr, F. Dulat, and B. Mistlberger, Phys. Rev. Lett. **125,** 051804 (2020).

[78] S. Forte, D. Napoletano, and M. Ubiali, Phys. Lett. B **751,** 331 (2015); **763,** 190 (2016); M. Bonvini, A. S. Papanastasiou, and F. J. Tackmann, J. High Energy Phys. 11 (2015) 196; M. Bonvini, A. S. Papanastasiou, and F. J. Tackmann, J. High Energy Phys. 10 (2016) 053.

[79] S. Dawson, A. Djouadi, and M. Spira, Phys. Rev. Lett. **77,** 16 (1996); R. V. Harlander and M. Steinhauser, Phys. Lett. B **574,** 258 (2003); J. High Energy Phys. 09 (2004) 066; R. V. Harlander and F. Hofmann, J. High Energy Phys. 03 (2006) 050; M. Mühlleitner and M. Spira, Nucl. Phys. **B790,** 1 (2008); R. Bonciani, G. Degrassi, and A. Vicini, J. High Energy Phys. 11 (2007) 095; G. Degrassi and P. Slavich, Nucl. Phys. **B805,** 267 (2008); J. High Energy Phys. 11 (2010) 044; M. Mühlleitner, H. Rzehak, and M. Spira, J. High Energy Phys. 04 (2009) 023; C. Anastasiou, S. Beerli, and A. Daleo, Phys. Rev. Lett. **100,** 241806 (2008); R. V. Harlander, F. Hofmann, and H. Mantler, J. High Energy Phys. 02 (2011) 055; G. Degrassi, S. Di Vita, and P. Slavich, J. High Energy Phys. 08 (2011) 128; Eur. Phys. J. C **72,** 2032 (2012).

[80] M. Mühlleitner, H. Rzehak, and M. Spira, Proc. Sci., RADCOR2009 (**2010**) 043Report No. DESY-PROC-2010-01.

[81] A. Djouadi and M. Spira, Phys. Rev. D **62,** 014004 (2000).

[82] W. Hollik, T. Plehn, M. Rauch, and H. Rzehak, Phys. Rev. Lett. **102,** 091802 (2009); T. Figy, S. Palmer, and G. Weiglein, J. High Energy Phys. 02 (2012) 105.

[83] S. Dittmaier, P. Häfliger, M. Krämer, M. Spira, and M. Walser, Phys. Rev. D **90,** 035010 (2014).

[84] S. Dittmaier, M. Krämer, A. Mück, and T. Schlüter, J. High Energy Phys. 03 (2007) 114; S. Dawson, C. B. Jackson, and P. Jaiswal, Phys. Rev. D **83,** 115007 (2011).

[85] A. Arbey, M. Battaglia, and F. Mahmoudi, Eur. Phys. J. C **72,** 1847 (2012).

[86] B. C. Allanach, Comput. Phys. Commun. **143,** 305 (2002).
[87] A. Djouadi, J. L. Kneur, and G. Moultaka, Comput. Phys. Commun. **176,** 426 (2007).
[88] S. Heinemeyer, W. Hollik, and G. Weiglein, Comput. Phys. Commun. **124,** 76 (2000).
[89] M. Mühlleitner, A. Djouadi, and Y. Mambrini, Eur. Phys. J. C **20,** 563 (2001); Comput. Phys. Commun. **168,** 46 (2005).
[90] F. Mahmoudi, Comput. Phys. Commun. **178,** 745 (2008); F. Mahmoudi, Comput. Phys. Commun. **180,** 1579 (2009); A. Arbey and F. Mahmoudi, Comput. Phys. Commun. **181,** 1277 (2010); A. Arbey, F. Mahmoudi, and G. Robbins, Comput. Phys. Commun. **239,** 238 (2019).
[91] G. Belanger, F. Boudjema, A. Pukhov, and A. Semenov, Comput. Phys. Commun. **180,** 747 (2009).
[92] M. Spira, arXiv:hep-ph/9510347.
[93] The ATLAS Collaboration, J. High Energy Phys. 04 (2019) 098.
[94] A. M. Sirunyan *et al.* (CMS Collaboration), J. High Energy Phys. 04 (2020) 188.
[95] R. Aaij *et al.* (LHCb Collaboration), Phys. Rev. D **105,** 012010 (2022).
[96] A. Arbey, M. Battaglia, F. Mahmoudi, and D. Martínez Santos, Phys. Rev. D **87,** 035026 (2013).
[97] Y. S. Amhis *et al.* (HFLAV Collaboration), Eur. Phys. J. C **81,** 226 (2021).
[98] T. Hurth, F. Mahmoudi, D. M. Santos, and S. Neshatpour, Phys. Lett. B **824,** 136838 (2022).
[99] The ATLAS, CMS and LHCb Collaborations, Reports No. LHCb-CONF-2020-002, No. CMS PAS BPH-20-003, No. ATLAS-CONF-2020-049.
[100] N. Aghanim *et al.* (Planck Collaboration), Astron. Astrophys. **641,** A6 (2020); **652,** C4(E) (2021).
[101] E. Aprile *et al.* (XENON Collaboration), Phys. Rev. Lett. **121,** 111302 (2018).
[102] J. Alwall, M. Herquet, F. Maltoni, O. Mattelaer, and T. Stelzer, J. High Energy Phys. 06 (2011) 128.
[103] T. Sjöstrand, S. Ask, J. R. Christiansen, R. Corke, N. Desai, P. Ilten, S. Mrenna, S. Prestel, C. O. Rasmussen, and P. Z. Skands, Comput. Phys. Commun. **191,** 159 (2015).
[104] S. Ovyn, X. Rouby, and V. Lemaitre, arXiv:0903.2225; J. de Favereau *et al.*, arXiv:1307.6346.
[105] A. L. Read, J. Phys. G **28,** 2693 (2002).
[106] The ATLAS Collaboration, J. High Energy Phys. 01 (2018) 055.
[107] The ATLAS Collaboration, Eur. Phys. J. C **78,** 293 (2018).
[108] The ATLAS Collaboration, Phys. Rev. Lett. **119,** 191803 (2017).
[109] The ATLAS Collaboration, Report No. ATLAS-CONF-2019-040.
[110] The ATLAS Collaboration, J. High Energy Phys. 12 (2017) 034.
[111] The ATLAS Collaboration, Phys. Rev. D **96,** 112010 (2017).
[112] The ATLAS Collaboration, J. High Energy Phys. 06 (2020) 046.
[113] The ATLAS Collaboration, J. High Energy Phys. 12 (2017) 085.
[114] The ATLAS Collaboration, Report No. ATLAS-CONF-2018-041.
[115] The ATLAS Collaboration, Eur. Phys. J. C **80,** 123 (2020).
[116] The ATLAS Collaboration, Eur. Phys. J. C **78,** 995 (2018).
[117] The ATLAS Collaboration, J. High Energy Phys. 01 (2018) 126.
[118] The ATLAS Collaboration, Phys. Lett. B **763,** 251 (2016).
[119] The ATLAS Collaboration, Report No. ATL-CONF-2021-053.
[120] The ATLAS Collaboration, Report No. ATL-PHYS-PUB-2018-054.
[121] J. de Blas, M. Cepeda, J. D'Hondt, R. K. Ellis, C. Grojean, B. Heinemann, F. Maltoni, A. Nisati, E. Petit, R. Rattazzi, and W. Verkerke, J. High Energy Phys. 01 (2020) 139.
[122] G. Aarons *et al.*, arXiv:0709.1893; H. Baer *et al.*, arXiv:1306.6352; E. Accomando *et al.*, arXiv:hep-ph/0412251; G. Weiglein *et al.*, Phys. Rep. **426,** 47 (2006); T. Abe *et al.*, arXiv:hep-ex/0106056; E. Accomando *et al.*, Phys. Rep. **299,** 1 (1998); A. Djouadi, Int. J. Mod. Phys. A **10,** 1 (1995); H. Murayama and M. Peskin, Annu. Rev. Nucl. Part. Sci. **46,** 533 (1996).
[123] J. A. Aguilar-Saavedra *et al.* (ECFA/DESY LC Physics Working Group), arXiv:hep-ph/0106315.
[124] T. Kuhl and K. Desch, Report No. LC-PHSM-2007-001.
[125] The CMS Collaboration, Report No. CMS-PAS-HIG-19-005.
[126] J. F. Gunion and H. E. Haber, Phys. Rev. D **67,** 075019 (2003); M. Carena, I. Low, N. R. Shah, and C. E. M. Wagner, J. High Energy Phys. 04 (2014) 015; M. Carena, H. E. Haber, I. Low, N. R. Shah, and C. E. M. Wagner, Phys. Rev. D **91,** 035003 (2015).